



Article

Pt(II) Complexes with a Novel Pincer N[^]C[^]N Ligand: Synthesis, Characterization, and Photophysics

Evgeniia E. Luneva, Daria O. Kozina, Anna V. Mozzhukhina, Vitaly V. Porsev , Anastasia I. Solomatina * and Sergey P. Tunik *

Institute of Chemistry, St. Petersburg State University, Universitetskii Av., 26, 198504 St. Petersburg, Russia; yevgeniyalunyo@gmail.com (E.E.L.); kozina.d@yandex.ru (D.O.K.); st101545@student.spbu.ru (A.V.M.); v.porsev@spbu.ru (V.V.P.)

* Correspondence: a.solomatina@spbu.ru (A.I.S.); sergey.tunik@spbu.ru (S.P.T.)

Abstract: A series of new platinum square planar complexes [Pt(NCN)L]^{+ / 0} with the pincer N[^]C[^]N cyclometallated ligand (NC(H)N = 1,3-bis(1-phenyl-1H-phenanthro[9,10-d]imidazol-2-yl)benzene) containing the following L: Cl⁻, acetonitrile, pyridine, dimethylaminopyridine, 2,6-dimethylphenylisocyanide, has been synthesized. Application of bridging acetate ion as L ligand allowed obtaining a binuclear [Pt(NCN)]₂OOCCH₃ complex. The bulky and rigid structure of N[^]C[^]N-ligand provokes instability of its pincer coordination that makes possible transformation of the molecular architecture to give a heteronuclear complex with the Pt-Ag-Pt coordination core. The composition and structure of the obtained compounds were characterized in solution and in the solid state using ESI mass-spectrometry, NMR spectroscopy, elemental analysis, and single-crystal XRD crystallography. The complexes luminesce in solid state, solution, and in polymeric matrix demonstrating moderate to bright emission at ca. 550 nm with quantum yields up to 22% and lifetime of excited state up to 22 μs. TD DFT computational approach together with analysis of the photophysical properties in different media reveals the predominant ligand-centered ³IL nature of the radiative excited state localized at the N[^]C[^]N-ligand. The ancillary ligand L demonstrates a minor influence on the energy of emission but affects dramatically emission efficiency and lifetime. The chloride complex displays dual (fluorescence and phosphorescent) luminescence due to labile coordination of an N-coordinated functionality that produces a dangling aromatic fragment, which gives emission from a singlet excited state.

Keywords: platinum; silver; pincer complexes; photophysics; polynuclear complex; dual emission



Citation: Luneva, E.E.; Kozina, D.O.; Mozzhukhina, A.V.; Porsev, V.V.; Solomatina, A.I.; Tunik, S.P. Pt(II) Complexes with a Novel Pincer N[^]C[^]N Ligand: Synthesis, Characterization, and Photophysics. *Inorganics* **2023**, *11*, 198. <https://doi.org/10.3390/inorganics11050198>

Academic Editors: Valentina Utochnikova and Pingwu Du

Received: 12 April 2023

Revised: 27 April 2023

Accepted: 29 April 2023

Published: 3 May 2023



Copyright: © 2023 by the authors. Licensee MDPI, Basel, Switzerland. This article is an open access article distributed under the terms and conditions of the Creative Commons Attribution (CC BY) license (<https://creativecommons.org/licenses/by/4.0/>).

1. Introduction

Platinum(II) complexes are commonly known as bright luminophores [1,2] and are widely used as emitters in OLEDs [3], sensors [4–6], and dyes for bioimaging in vitro [7–9] and in vivo [10–12]. The square planar structure of such compounds determines a number of their unique properties related to photophysical performance, such as aggregation-induced emission, mechano-, and solvatochromism [13,14], which make possible a wide range of applications including biomedicine [15,16]. Due to the planar structure and the presence of d_{z2} orbitals perpendicular to the plane, platinum complexes are prone to the formation of π–π stacking [1,8,13,17], intermolecular and intramolecular short Pt–Pt contacts [18], halogen bonding [19], and tend to afford heterometallic complexes with Pt^{II} → M dative bond or metal-only Lewis pairs (MOLPs) [20–23]. One of the ways to achieve advantageous photophysical characteristics of platinum(II) complexes consists in the introduction of the ligands with strong sigma-donor and π-acceptor properties into the coordination environment, thus reducing the availability of non-radiative relaxation through d-d* excited state [24]. The cyclometallated N[^]C[^]N-pincer ligands, which contain C–donor functions, match well this requirement and usually ensure a highly efficient luminescence [17,25,26]. It is also suggested that due to the steric rigidity of the pincer

complexes, they do not undergo distortions in the excited state [26] that minimize Huang–Rhys factor [27,28] and give lower magnitudes of the non-radiative relaxation rate constants.

Among the complexes with cyclometallated aromatic N[∧]C[∧]N-ligands, the compounds based on 1,3-bis(pyrid-2-yl)benzene are the most studied [17,29–31] including investigation of the effects caused by variations of the ligands in the fourth position at the platinum center *trans* to cyclometallated carbon, which affords a change in the nature of the excited state [32] and a significant increase in the emission quantum yield [33]. Their structural and electronic analogs based on 1,3-bis(imidazol-2-yl)benzene are much less explored [34–37]. The studied complexes of this type with the chloride ligand in the fourth vacancy are known to exhibit luminescence at 510–550 nm [34,35] with well-structured emission bands that indicate a significant contribution of the ligand centered (³LC) character to the emissive excited state [35]. The substitution of the chloride ligand in the coordination sphere of platinum for isocyanides leads to only a slight hypsochromic shift of the emission band to 490 nm [38], while alkynes practically do not affect the emission energy even if their structure contains conjugated aromatic systems as well as donor and acceptor groups [36,37,39–42]. However, the effect of the further development of the conjugated aromatic structure of the cyclometallated ligand based on 1,3-bis(imidazol-2-yl)benzene on the photophysical performance has not yet been reported in the literature. Therefore, herein, we focused on studying the effect of the π -system expansion of the cyclometallated ligand and the choice of the L-ligand (different nature and ligand strength) on the structure and photophysical properties of N[∧]C[∧]N-Pt-L complexes of this type (Figure 1).

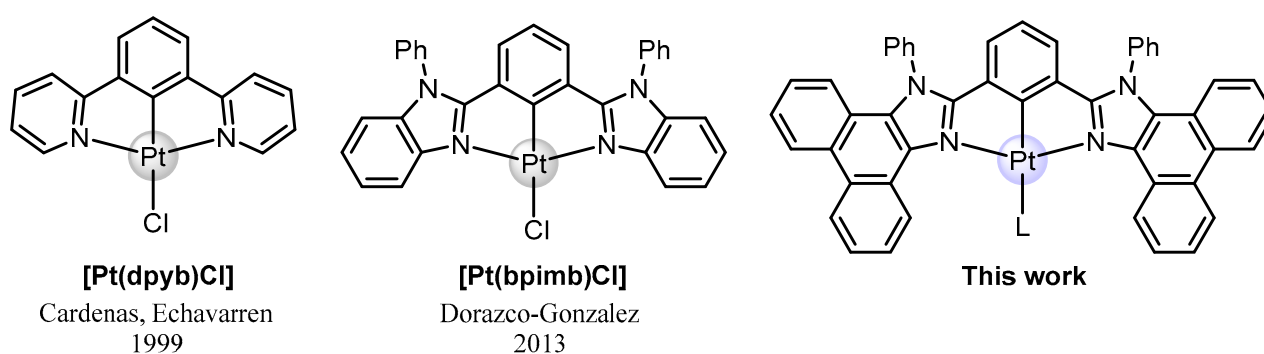


Figure 1. The previously reported compounds [30,34] and the complexes under study in this work.

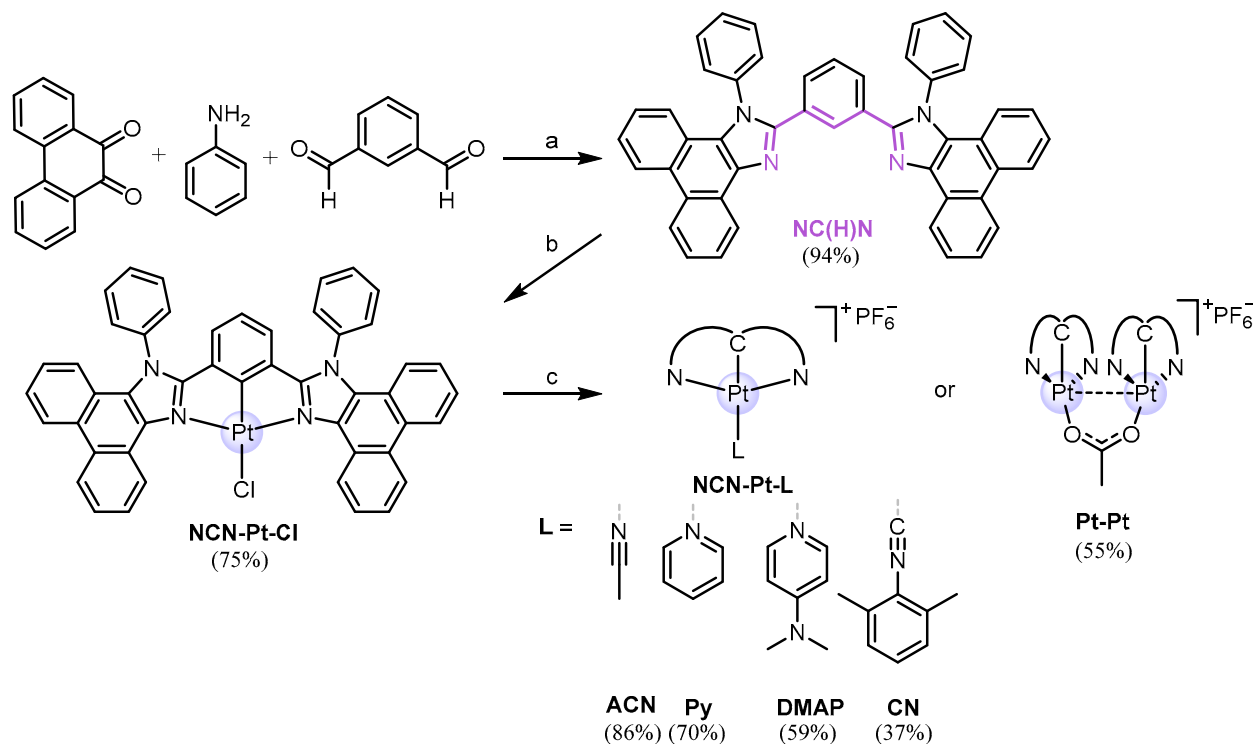
It has been shown that the nature of the emissive excited state of the studied complexes is determined by the N[∧]C[∧]N ligand, but emission efficiency and lifetime are strongly dependent on the nature of the lateral ligand L (Figure 1). Moreover, the choice of L leads to variations in the structural motif of the products obtained. The bulky aromatic π -system of cyclometallated ligand leads to the distortion of the square planar structure, which results in the lability of the pincer chelate. Depending on the degree of the distortion and ligand field strength of L, the complexes are prone to partial de-coordination of the pincer chelate in diluted organic solutions and give an unusual polynuclear complex in reaction with silver(I) cation.

2. Results and Discussion

2.1. Design, Synthesis, and Characterization of Mononuclear and Polynuclear Complexes

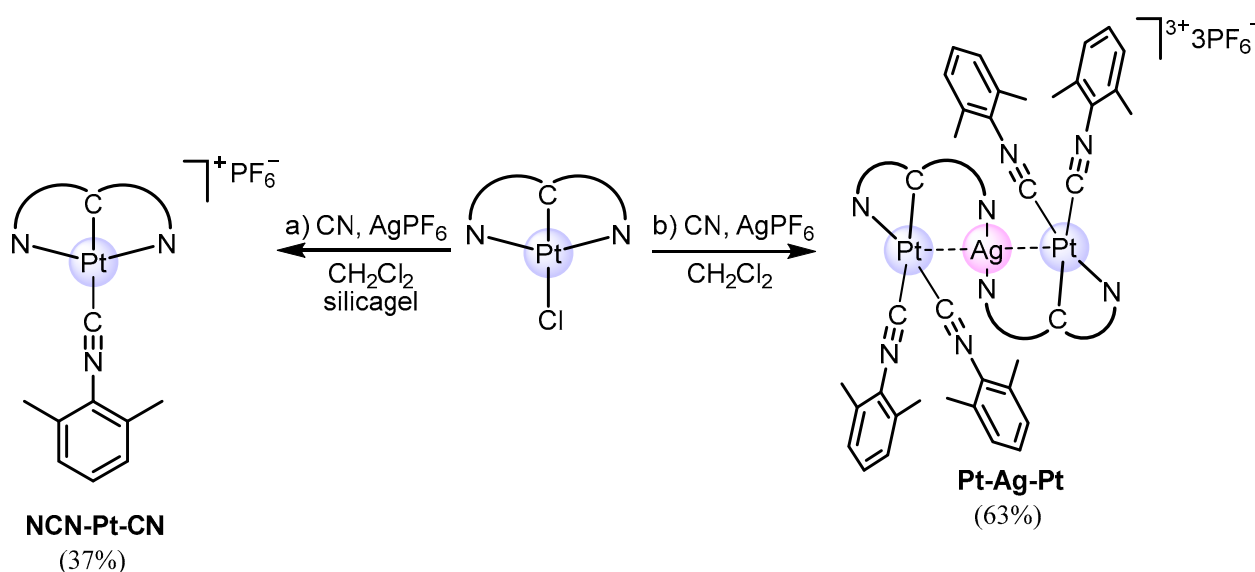
A convenient approach to the preparation of N[∧]C[∧]N-cyclometallated proligands is the multicomponent Debus–Radzizhevsky reaction enabling the formation of the imidazole ring [43,44]. This method makes it possible to obtain versatile organic molecules, which are known as effective luminophores in the visible and near-infrared spectral ranges [45–47]. The N[∧]C[∧]N-proligand NC(H)N was obtained similarly to the literature method [48,49] by heating a mixture of isophthalic aldehyde and phenantren-9,10-dione in the presence of an excess of aniline and ammonium acetate in acetic acid at 70°C (Scheme 1, reaction

a). In the course of the reaction, the target product precipitates as a white solid which simplifies the isolation of the product and subsequent purification. The platinum chloride complex **NCN-Pt-Cl** was then obtained with the standard cyclometallation reaction [34,50] by boiling the proligand and K_2PtCl_4 in degassed acetic acid (Scheme 1, reaction b). The reaction is rather slow to give the preparative yield of only 22% after 4 days, whereas boiling for 2 weeks increased the yield up to 75%.



Scheme 1. Synthesis of mononuclear complexes and binuclear **Pt-Pt** compound: (a) AcOH, AcONH₄, 70 °C, 3 h; (b) AcOH, reflux, 2 weeks; (c) **NCN-Pt-ACN**: acetonitrile, AgPF₆, RT; **NCN-Pt-Py**: pyridine, DCM, AgPF₆, RT; **NCN-Pt-DMAP**: dimethylaminopyridine, DCM, AgPF₆, RT; **NCN-Pt-CN**: 2,6-dimethylphenylisocyanide, DCM, AgPF₆, RT; **Pt-Pt**: acetic acid, ethyl acetate, AgPF₆, RT.

Substitution of chloride for the other ligands with different electron-donating and accepting properties: acetonitrile, pyridine, dimethylaminopyridine, 2,6-dimethylphenylisocyanide (Scheme 1, reaction c), in the presence of excess of AgPF₆ gave the corresponding mononuclear complexes: **NCN-Pt-ACN**, **NCN-Pt-Py**, **NCN-Pt-DMAP**, **NCN-Pt-CN**. In the case of the bidentate acetate ligand, the binuclear **Pt-Pt** compound formed. The products were obtained in moderate to high yields as pale to bright yellow crystalline compounds. It has been found that the reaction of the starting chloride complex **NCN-Pt-Cl** with isocyanide in the presence of silver salt gave another product, which converts to the target **NCN-Pt-CN** only after chromatography on silica (Scheme 2a). However, avoiding the chromatographic purification, it was possible to isolate a heterometallic polynuclear compound **Pt-Ag-Pt** (Scheme 2b). This compound was obtained in good yield as light yellow crystals after optimization of the synthetic procedure.



Scheme 2. Two types of products were obtained in reaction of NCN-Pt-Cl and 2,6-dimethylphenylisocyanide.

The molecular structures of the complexes obtained, NCN-Pt-ACN , NCN-Pt-Py , NCN-Pt-DMAP , NCN-Pt-PCN , Pt-Pt , and Pt-Ag-Pt , were determined in the solid state by means of single crystal X-ray diffraction crystallography (Figures 2, 3 and S1); selected structural parameters are provided in ESI, Tables S1 and S2. The neutral complex NCN-Pt-Cl and cationic NCN-Pt-L demonstrate very similar structural arrangements. The pincer $\text{N}^{\wedge}\text{C}^{\wedge}\text{N}$ ligand is coordinated in a tridentate manner to the Pt(II) ion forming two five-membered metallocycles. The fourth vacancy in the metal coordination sphere is occupied either by chloride or neutral monodentate ligand L. The square planar environment of the Pt(II) ion is considerably distorted due to bulky phenantroimidazolium moieties of the cyclometalated ligand and its repulsive interaction with the ligands in the *trans*-position to cyclometalated carbon. Due to rigidity of the $\{\text{Pt}(\text{N}^{\wedge}\text{C}^{\wedge}\text{N})\}$ fragment, this structural motif does not leave enough space for the fourth ligand (L), and the C-Pt-L angle deviates from 180° (see Table S2). The strongest distortion is observed in the case of $\text{L} = \text{Cl}^-$ and 2,6-dimethylphenylisocyanide, the repulsion between L and fragments of the pincer ligand results in displacement of L from the $\{\text{Pt}(\text{N}^{\wedge}\text{C}^{\wedge}\text{N})\}$ plane giving the C-Pt-L angles of 156° and 160° , respectively. In the case of NCN-Pt-ACN , smaller distortion is observed (C-Pt-L angle = 164°) due to lower cone angle of acetonitrile compared to chloride and isocyanide. The geometry of NCN-Pt-Py differs from the other complexes (see Figure S1), phenanthroline aromatic fragments are forced to be located above and below the metal coordination plane while the nitrogen atom of pyridine ligand is placed within the plane providing the lowest distortion with C-Pt-L angle of 178° . The bond lengths between platinum ion and coordinated atoms of the ligand are typical for this type of compounds [34–36,51] and show no systematic dependence on the electronic properties of L. In the crystal cell, the complexes demonstrate π - π interactions between metalated ligands. However, the rigid $\text{N}^{\wedge}\text{C}^{\wedge}\text{N}$ -ligand bearing two phenyl groups oriented perpendicular to the ligand aromatic system together with out of plane position of the lateral L-ligand prevent strong intermolecular interactions and short metal-metal contacts in the crystal structure (Figure S1).

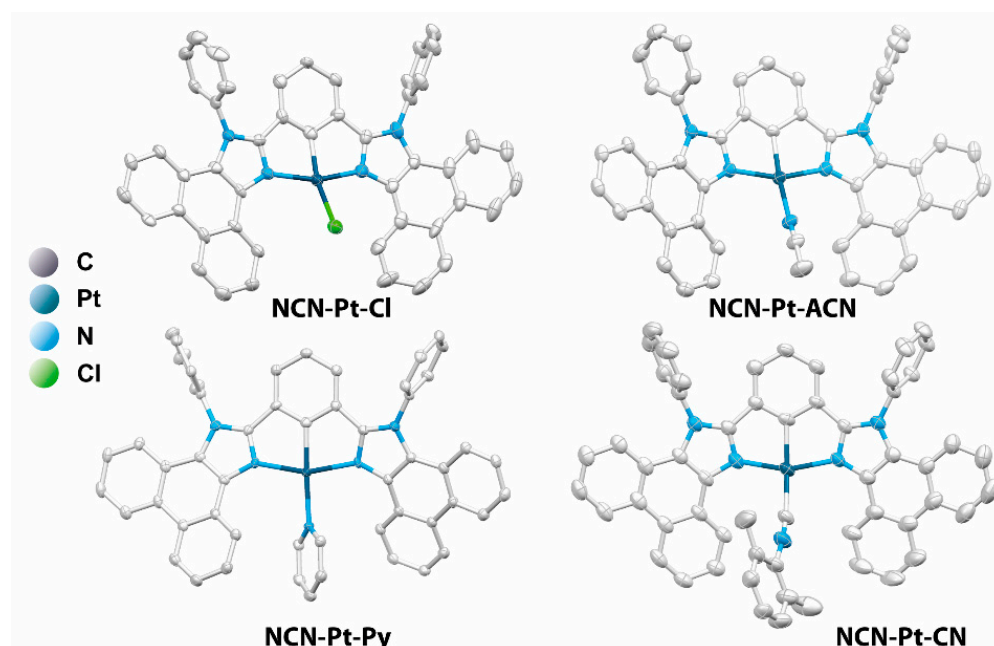


Figure 2. Perspective view of molecular ions of complexes in the solid state showing *thermal ellipsoids* at the 50% *probability* level. Hydrogen atoms and counterions are omitted for clarity.

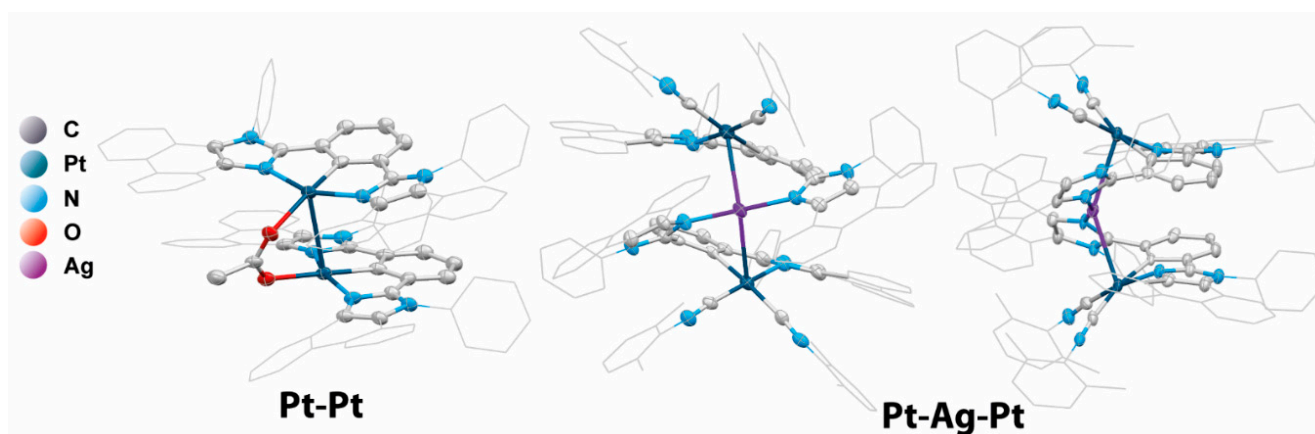


Figure 3. Perspective view of **Pt-Pt** and **Pt-Ag-Pt** molecular backbones in the solid state showing *thermal ellipsoids* at the 50% *probability* level. Hydrogen atoms and counterions are omitted for clarity. Some groups are shown as wireframes to clarify general structural motifs.

The binuclear complex **Pt-Pt** is formed from two $\{Pt(N^{\wedge}C^{\wedge}N)\}$ moieties joined together by the bridging acetate ligand (Figure 3). In this configuration, platinum ions form direct metallophilic bonding with the distance between platinum atoms equal to 3.1396(3) Å, which is less than the sum of the Van der Waals radii and typical of platinum complexes exhibiting strong Pt...Pt interaction and π - π stacking [52]. Analogously to the mononuclear complexes, the oxygens of the acetate ligand occupy the fourth vacancy and are considered withdrawn from the $\{Pt(N^{\wedge}C^{\wedge}N)\}$ plane (C-Pt-O angles = 168 and 176°). The cyclometallated fragments are located against each other, but the fragments are slightly shifted relative to each other to avoid repulsion between phenyl substituents.

The complicated architecture of the heterometallic **Pt-Ag-Pt** compound found in the solid state (Figure 3) is formed through reorganization of the coordination sphere of two $\{Pt(N^{\wedge}C^{\wedge}N)\}$ moieties in the presence of silver ion and isocyanides. In **Pt-Ag-Pt**, the square planar arrangement of each platinum ion is formed by two isocyanide ligands and an $N^{\wedge}C$ -chelate from the pincer ligand. Silver ion bridges two $\{Pt(N^{\wedge}C)\}$ moieties by binding with de-coordinated imidazole nitrogens of the tridentate ligand to form the structural

pattern shown in Scheme 2 and Figure 3. The heterometallic core is additionally stabilized by the $\text{Pt}^{\text{II}}(d_{z^2}) \rightarrow \text{Ag}^{\text{I}}$ dative bonds. The Pt-Ag distance is about 2.97 Å, and the Pt-Ag-Pt angle is 155°. These values are close to the structural parameters found in analogous heterometallic compounds [21].

The compounds obtained have been completely characterized by ESI⁺ mass spectrometry, NMR spectroscopy, and elemental analysis (Figures S2–S14). The ESI⁺ mass spectra of all the mononuclear complexes studied (Figure S2) display one dominating signal of the $[\text{Pt}(\text{N}^{\wedge}\text{C}^{\wedge}\text{N})]^+$ cation and relatively weak signals from $[\text{Pt}(\text{N}^{\wedge}\text{C}^{\wedge}\text{N})\text{L}]^+$, indicating relative lability of the Pt-L bond. The binuclear complex **Pt-Pt** and heterometallic complex **Pt-Ag-Pt** similarly are not stable under the conditions of the mass spectroscopic experiment and show the major signals in their mass spectra corresponding to the $[\text{Pt}(\text{N}^{\wedge}\text{C}^{\wedge}\text{N})]^+$ and $[\text{Pt}(\text{N}^{\wedge}\text{C}^{\wedge}\text{N})(\text{CN})_2]^+$ stoichiometry, respectively. The isotopic patterns of the obtained signals fit well with the calculated ones. Signal assignment in the ¹H NMR spectra was performed using ¹H-¹H COSY and NOESY spectroscopies (Figures S3–S14). The intramolecular “through space” nonbonding contacts between protons of the lateral and pincer ligands found in the NOESY spectra evidenced that the fourth ligand remains in the coordination sphere of the complexes (Figures S8, S10, and S13). Thus, in solution, the mononuclear complexes and the binuclear **Pt-Pt** retain the molecular structure found in the solid state.

It should be noted that the chloride complex **NCN-Pt-Cl** demonstrates the broadening of some signals in the proton NMR spectrum observed at a low concentration of the complex in DMSO-d₆ and more pronounced in CD₂Cl₂ (Figures S5 and S6). The signals related to the protons of the phenanthroimidazol moieties, which are closest to the platinum ion and the chloride ligand, are mainly subjected to the broadening. This may indicate the presence of intramolecular dynamics in solution due to either relatively weak bonding of the chloride ligand or because of labile coordination of the pyridine fragments associated with the steric tension of the entire coordination environment, *vide supra*.

The data of the ¹H-¹H COSY and NOESY correlation NMR experiments (Figure S14) clearly demonstrate that in solution the heterometallic **Pt-Ag-Pt** complex keeps unchanged the polynuclear structural motif revealed in the crystal cell. The spectrum shows one set of signals from nonsymmetric cyclometalated ligands and two sets of the signals corresponding to isocyanide ligands coordinated to platinum and silver ions. This observation indicates the presence of the second-order rotational axis passing through the silver ion and the center of the Pt-Pt distance that fits completely the C₂ symmetry point group found in the solid state (Figure 3). Moreover, short nonbonding intramolecular contacts observed in the solid-state structure were also detected by the ¹H-¹H NOESY spectroscopy that indicated structural rigidity of this polynuclear molecule in the fluid phase.

2.2. Photophysical Properties and Computational Studies

The complexes obtained demonstrate emission in the solid state, in the polymer matrix of poly(methyl methacrylate) (PMMA, 2%), and in solution. Photophysical characteristics of the compounds in dichloromethane (DCM) solution are summarized in Table 1, absorption and emission spectra are shown in Figure 4.

Table 1. Photophysical properties of complexes in CH₂Cl₂.

N ^o	$\lambda_{\text{abs}}, \text{nm}$ ($\epsilon \times 10^{-3}, \text{M}^{-1}\text{cm}^{-1}$)	$\lambda_{\text{em}}, \text{nm}$ 298 K, (77 K)	$\tau_{\text{obs}}^{\text{a}}$ (aer/deg) ^b , μs	Φ (aer/deg) ^b , %	$k_{\text{r}}^{\text{c}}, \text{s}^{-1}$	$k_{\text{nr}}^{\text{d}}, \text{s}^{-1}$
NC(H)N	260 (104), 320 (32), 345 (22), 362 (20)	373, 392, 410sh, 440sh	1.82 ns @ 450 nm fl: 0.0041	30 fl: 3.03	1.65×10^8	3.85×10^8
NCN-Pt-Cl	257 (78), 270sh (61), 300sh (27), 315sh (23), 345sh (18), 356sh (16), 376 (13), 398 (14), 424 (18)	fl: 397, 416, 440, ph: 525, 568, 615sh (526, 570, 622)	@ 450 nm ph: 0.053/0.060 @ 600 nm	@ 420 nm ph: 0.56/0.87 @ 600 nm	*	*
NCN-Pt-ACN	247 (67), 270sh (44), 310sh (16), 345sh (18), 358sh (13), 395 (16), 420 (17)	523, 564, 605sh (522, 564, 613, 670sh)	0.55/2.27	0.75/3.6	0.016×10^6	0.425×10^6
NCN-Pt-Py	258 (55), 310sh (18), 364sh (13), 384sh (13), 393sh (13), 405 (13), 420 (9.1)	523, 564, 605sh	0.32/0.93	0.39/2.3	0.025×10^6	1.05×10^6
NCN-Pt-DMAP	261 (61), 270sh (58), 305sh (26), 328sh (15), 340sh (12), 368 (13), 388 (14), 409 (16), 420sh (6.4)	524, 564, 605sh	0.36/1.96	0.35/1.14	0.0058×10^6	0.50×10^6
NCN-Pt-CN	259 (60), 300sh (24), 330sh (17), 345sh (14), 376 (15), 391 (14), 405sh (11)	524, 564, 605sh	0.20/0.96	0.10/0.18	0.019×10^6	1.04×10^6
Pt-Pt	260 (60), 305sh (20), 325sh (14), 370sh (13), 385 (14), 407sh (15), 420sh (5.6)	525, 565, 605sh	0.61/8.54	0.67/9.02	0.011×10^6	0.11×10^6
Pt-Ag-Pt	260 (132), 300sh (47), 330sh (29), 353 (18), 390sh (11)	550sh, 578, 630sh (525, 565, 610, 670sh)	1.57/10.74	0.31/1.6	0.0015×10^6	0.09×10^6

^a Lifetime decays were measured in emission maximum with excitation at 355 nm, the value is shown as averaged lifetime of biexponential fit $\tau_{\text{obs}} = (A_1\tau_1^2 + A_2\tau_2^2)/(A_1\tau_1 + A_2\tau_2)$;

^b aer—aerated solution, deg—degassed solution; ^c k_{r} values were estimated for deaerated conditions as Φ/τ . ^d k_{nr} values were estimated for deaerated conditions as $(1-\Phi)/\tau$. * The constants cannot be calculated correctly, as the emission spectra contains two components and their lifetime and quantum yields values were estimated with some assumptions.

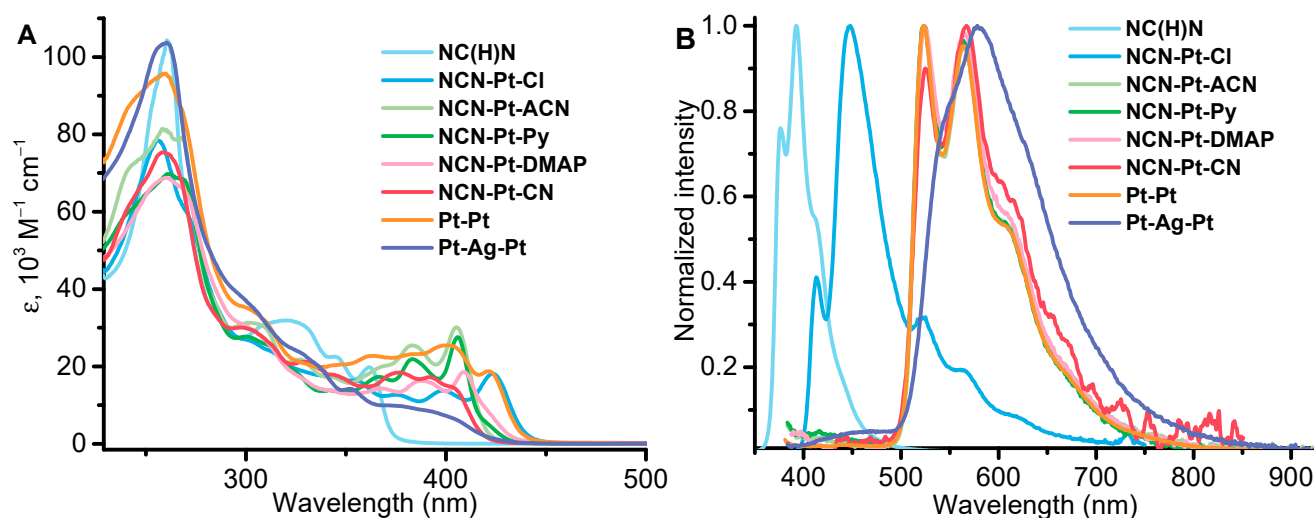


Figure 4. Absorption (A) and emission (B) spectra of the proligand and complexes in DCM, concentration 5×10^{-5} M, RT.

In dichloromethane (DCM), the proligand and complexes display strong absorption bands at ca. 250 nm and a series of shoulders located between 300 and 350 nm (Figure 4A). These features can be ascribed to the $\pi-\pi^*$ transitions in the aromatic systems of proligand, pincer and lateral ligands in the complexes. In addition, the complexes also demonstrate long wavelength absorption between 350 and 450 nm with pronounced vibrational structure observed for all complexes excluding **Pt-Ag-Pt**. According to the previously reported data [35] for closely related compounds and our DFT calculation results (Figures 5 and S21–S24, Table S3–S12), the low energy absorption may be assigned to metal-disturbed ligand centered (1LC) transitions in the cyclometallated fragment with some admixture of ligand(L)-to-ligand($N^{\wedge}C^{\wedge}N$) (1LLCT) and metal-to-ligand($N^{\wedge}C^{\wedge}N$) (1MLCT) charge transfers.

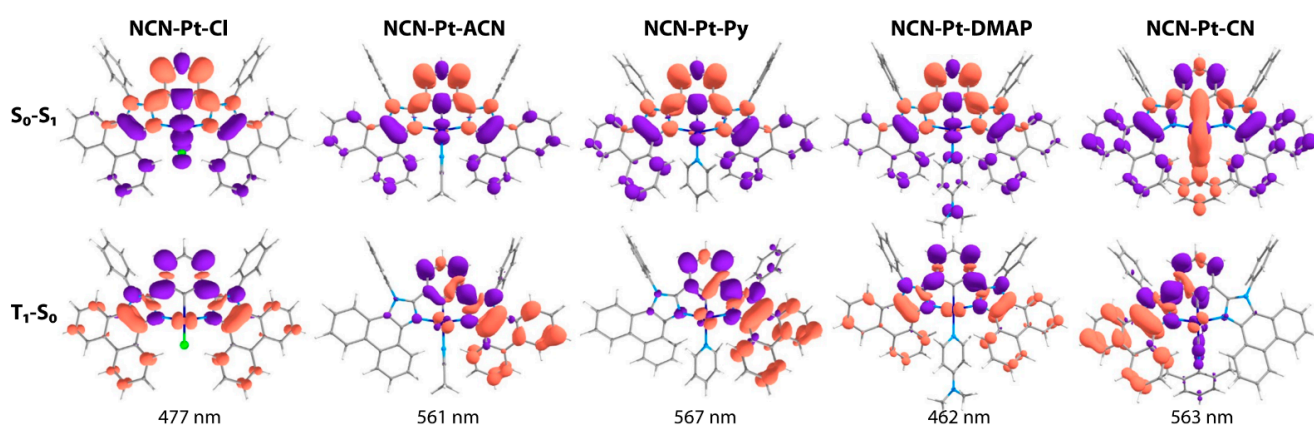


Figure 5. Electron density variations upon T_1-S_0 emission processes for mononuclear complexes **NCN-Pt-L**. Violet and terracotta colors denote the depletion and increase in electron density, respectively. The energy of vertical T_1-S_0 transition is denoted under corresponding picture.

All studied compounds are emissive in DCM solution at room temperature (Figure 4B). The proligand, **NC(H)N**, display rather strong fluorescence (quantum yield, Φ , 30%) with vibronically structured band at 392 nm and short lifetime of 1.82 ns. Its profile and energy of emission as well as absorption properties closely resemble other phenanthro[9,10-D]imidazole congeners [49] indicating the major role of this aromatic system in the photophysics.

The mononuclear **NCN-Pt-L** complexes, except for **NCN-Pt-Cl**, demonstrate nearly identical structured emission band (first maxima at 525 nm) with vibronic spacing of ca. 1350–1400 cm^{-1} (see Figures 4B and S16) that is typical for the family of $\text{N}^{\wedge}\text{C}^{\wedge}\text{N}$ -cyclometallated platinum(II) emitters [17,35]. The emission quantum yields and lifetimes display strong dependence on the concentration of oxygen in solution, indicating the triplet nature of the emission, i.e., phosphorescence (see Table 1, Figure S19). According to the results of TD DFT calculations (Figure 5 and Tables S6, S8, S10 and S12), the complexes' emissive excited states can be assigned to the metal disturbed ^3LC phosphorescence located at the aromatic system of the pincer ligand with a minor admixture of $^3\text{MLCT}/^3\text{LLCT}$ characters. The minor contribution of the lateral ligand L into emissive transitions results in the minimal effect of the ligands' nature on the emission energy of these complexes. Interestingly, the emission band of the binuclear complex **Pt-Pt** displays the emission profile, which completely coincides with those of the mononuclear complexes that point to essentially similar nature/energy of its emissive excited state. It is worth mentioning that the presence of Pt-Pt bonding (found in the **Pt-Pt** solid-state structure) usually provokes an increase in the LUMO energy thus reducing the gap between the emissive triplet and ground state [13]. The similarity of the **Pt-Pt** emission band to those of the mononuclear emitters indicates that the short Pt-Pt contact found in the crystal cell of the binuclear complex, *vide supra*, is either completely broken or partially elongated in solution and does not show any influence on the nature of excited state and emission energy.

The mononuclear **NCN-Pt-Cl** complex shows considerably more complicated photophysical behavior compared to the other mononuclear congeners (Figure 6, Table 1). Upon excitation in the low energy absorption band at ca. 420 nm (DCM solution, room temperature), the compound demonstrates a vibronically structured emission band, which is very similar to those observed for the other mononuclear complexes, see Table 1 and Figures 4 and 6. However, the observed phosphorescence features low quantum yield, short lifetime, and weak sensitivity to oxygen that differ from the data obtained for the other mononuclear complexes. These observations point to strong emission quenching in this complex that may be explained by an effective thermal population of nonemissive dd^* excited states from the long-lived T_1 . The situation is typical for the platinum complexes upon substitution of strong field ligands (σ -donors, π -acceptors) for weak-field ligands, such as chloride (σ, π -donors) [24,53–57].

Quite unexpectedly, the higher excitation of **NCN-Pt-Cl** in solution at 365 nm gave a fluorescence band at ca. 430 nm with substantially higher emission intensity compared to the phosphorescent one, which in this case appeared as a shoulder at the long wavelength tail of the fluorescence band, Figure 6. Upon cooling to 77 K, the intensity of the phosphorescence band dramatically increases whereas the fluorescence band remains unaffected (Figures 6 and S15). The higher-energy emission band appears in freshly prepared solutions of thoroughly purified samples in different solvents, including DCM, acetone, DMSO, acetonitrile, and 1,2-dichloroethane and therefore it has to be attributed to the complex itself, not to an impurity. The presence of this fluorescence can be explained by the existence of an equilibrium between **NCN-Pt-Cl** and a product of its rearrangement in solution. This product, presumably, is a complex with a partly de-coordinated $\text{N}^{\wedge}\text{C}^{\wedge}\text{N}$ ligand bearing one dangling phenylphenanthro[9,10-D]imidazole moiety, which can be a site of the singlet chromophore. De-coordination of this moiety can be evidently forced by steric hindrance clearly observed in the solid-state structure of this complex that has been also confirmed by the NOESY NMR spectra, *vide supra*. The broken bonding to the metal center considerably diminishes spin-orbit coupling due to limited interaction of the organic fragment π -orbitals and d-orbitals of metal atom thus provoking emission from a singlet excited state, which strongly competes with intersystem crossing into an emissive triplet. The **NCN-Pt-Cl** is not a unique example of dual singlet-triplet emission in square planar platinum complexes [58–61], where the effect of platinum atom orbitals onto organic chromophores is minimized due to one or another reason. The ligand fragment dissociation is not substantially stabilized by solvent coordination; therefore, the reaction equilibrium is

primarily shifted to the starting **NCN-Pt-Cl** complex generating only a minor amount of the product, which cannot be detected using NMR spectroscopy also because of the fast exchange rate between these two states of the complex. The hypothesis on the equilibrium is also supported by the broadening of some signals in the NMR spectrum discussed, see description of NMR data above. Upon cooling the **NCN-Pt-Cl** solution in liquid nitrogen, the thermal population of the non-emissive dd states is completely suppressed which gives a strong enhancement of the phosphorescence observed in the frozen solution, Figure S15.

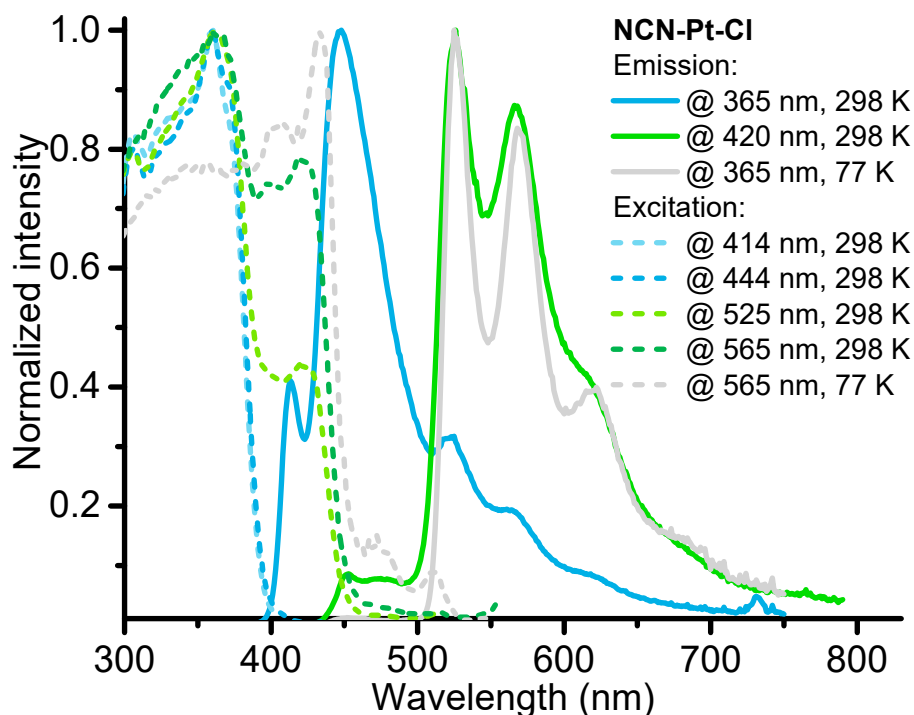


Figure 6. Excitation (dashed line) and emission (solid line) spectra **NCN-Pt-Cl** in DCM at RT and 77 K, $c = 1 \times 10^{-4}$ M.

The photophysical properties of the heterometallic trinuclear **Pt-Ag-Pt** complex differ from those of the homometallic complexes described above (see Table 1 and Figures 4 and 7). The absorption spectrum of the complex in DCM demonstrates a strong high energy band at 260 nm and broad low energy absorption extended down to ca. 425 nm (Figure 4). In solution at ambient temperature, **Pt-Ag-Pt** displays a yellow–orange structureless emission band with a maximum at 578 nm (see Table 1). Lifetime in the microsecond domain, high Stokes shift, and quenching of the emission in aerated solution additionally prove the triplet nature of the excited state. In the glassy solvent at 77 K, the emission band displays a slight blueshift for 13 nm together with the appearance of a fine structure with a vibrational spacing of ca. 1350 cm^{-1} . Based on these observations, together with the literature data for the related compounds [22,62] it is possible to suggest the $^3\text{IL} (\text{N}^{\wedge}\text{C}^{\wedge}\text{N})$ character dominates in the emissive transition with some admixture of the $^3\text{MLCT}$ or $^3\text{LL}'\text{CT}$ states.

In the solid state and in PMMA films, all the studied complexes show moderate to intense room temperature photoluminescence (Table 2, Figures 8, S17, S18 and S20). The emission spectra of the mononuclear **NCN-Pt-L** complexes display band profiles that closely resemble those observed in the solution (Figure 8A,B). The position of the maxima, the relative intensity of peaks, and the broadness of the spectra only slightly vary in the different media. Therefore, in the rigid polymer matrix and in the solid state, the nature of the emissive excited state remains unchanged demonstrating the major contribution of the $^3\text{IL} (\pi\pi^*, \text{N}^{\wedge}\text{C}^{\wedge}\text{N})$ character. These findings are in line with the major features of the complexes' molecular packing in crystal cell (see Figure S1), namely, no short contacts

or direct metal–metal interactions were observed ensuring a minor packing effect on the photophysical properties.

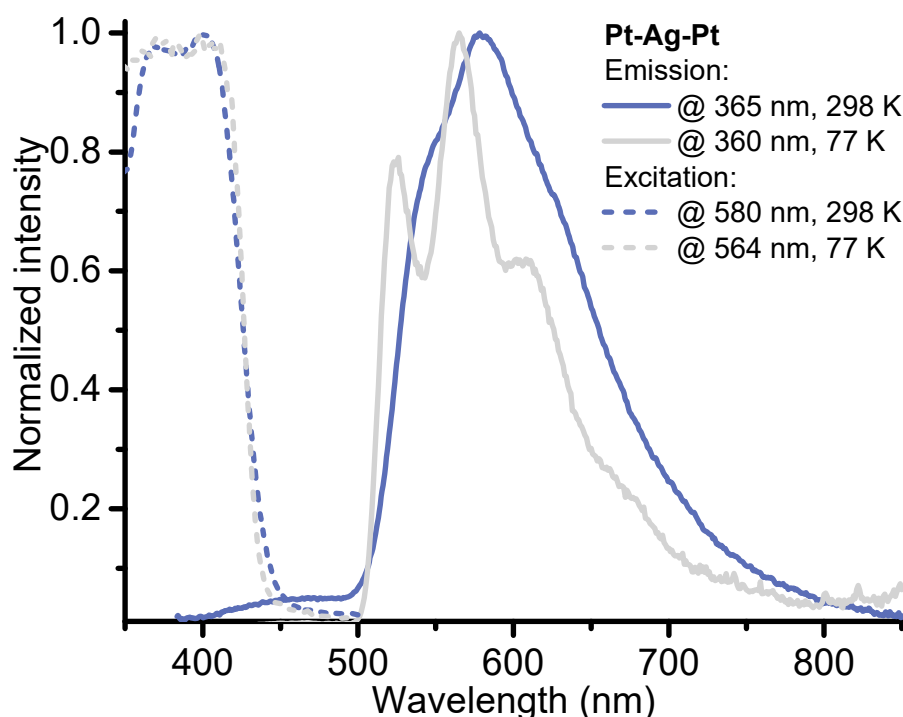


Figure 7. Excitation (dashed line) and emission (solid line) spectra **Pt-Ag-Pt** in DCM at RT and 77 K, $c = 1 \times 10^{-4}$ M.

Table 2. Photophysical properties of complexes in the solid state and in PMMA (2%), 298 K.

N ^o	Medium	λ_{ex} , nm	λ_{em} , nm	τ_{obs}^a , μ s	Φ , %	k_r^b , $\times 10^4$ s ⁻¹	k_{nr}^c , $\times 10^4$ s ⁻¹
NCN-Pt-Cl	solid state	435, 477, 510	523, 566, 616, 668sh	0.21	2.1	10.05	468.42
	PMMA	377, 400, 419	527, 568, 610sh, 675sh	5.4	12	2.24	16.40
NCN-Pt-ACN	solid state	422, 435, 477, 510	524, 566, 611, 668sh	1.2	4.7	4.02	81.45
	PMMA	368, 386, 407	535, 567, 625sh	10.5	11	1.05	8.49
NCN-Pt-Py	solid state	423, 477, 508	520, 566, 605sh	1.9	3.8	2.05	51.80
	PMMA	367, 384, 406	525, 560, 610sh	12.1	15	1.24	7.05
NCN-Pt-DMAP	solid state	405, 416, 477, 508	524, 566, 608, 668sh	2.6	12	4.70	34.50
	PMMA	370, 393, 414	530, 567, 620sh	8.5	12	1.41	10.34
NCN-Pt-CN	solid state	429, 477, 510	525, 567, 608, 670sh	0.99	1.4	1.41	99.30
	PMMA	370, 395, 405	523, 562, 610sh	15.5	13	0.84	5.62
Pt-Pt	solid state	440, 477, 503	562, 595, 645sh	0.71	1.8	2.53	137.92
	PMMA	366, 385, 407	520, 560, 610sh	11.5	14	1.21	7.46
Pt-Ag-Pt	solid state	403, 500	576	8.2	9	1.10	11.08
	PMMA	370, 395sh	529sh, 562, 610sh	22.2	22	0.99	3.51

^a Lifetime decays were measured in emission maximum with excitation at 355 nm, the value is shown as averaged lifetime of biexponential fit $\tau_{obs} = (A_1\tau_1^2 + A_2\tau_2^2)/(A_1\tau_1 + A_2\tau_2)$; ^b k_r values were estimated as Φ/τ ; ^c k_{nr} values were estimated as $(1-\Phi)/\tau$.

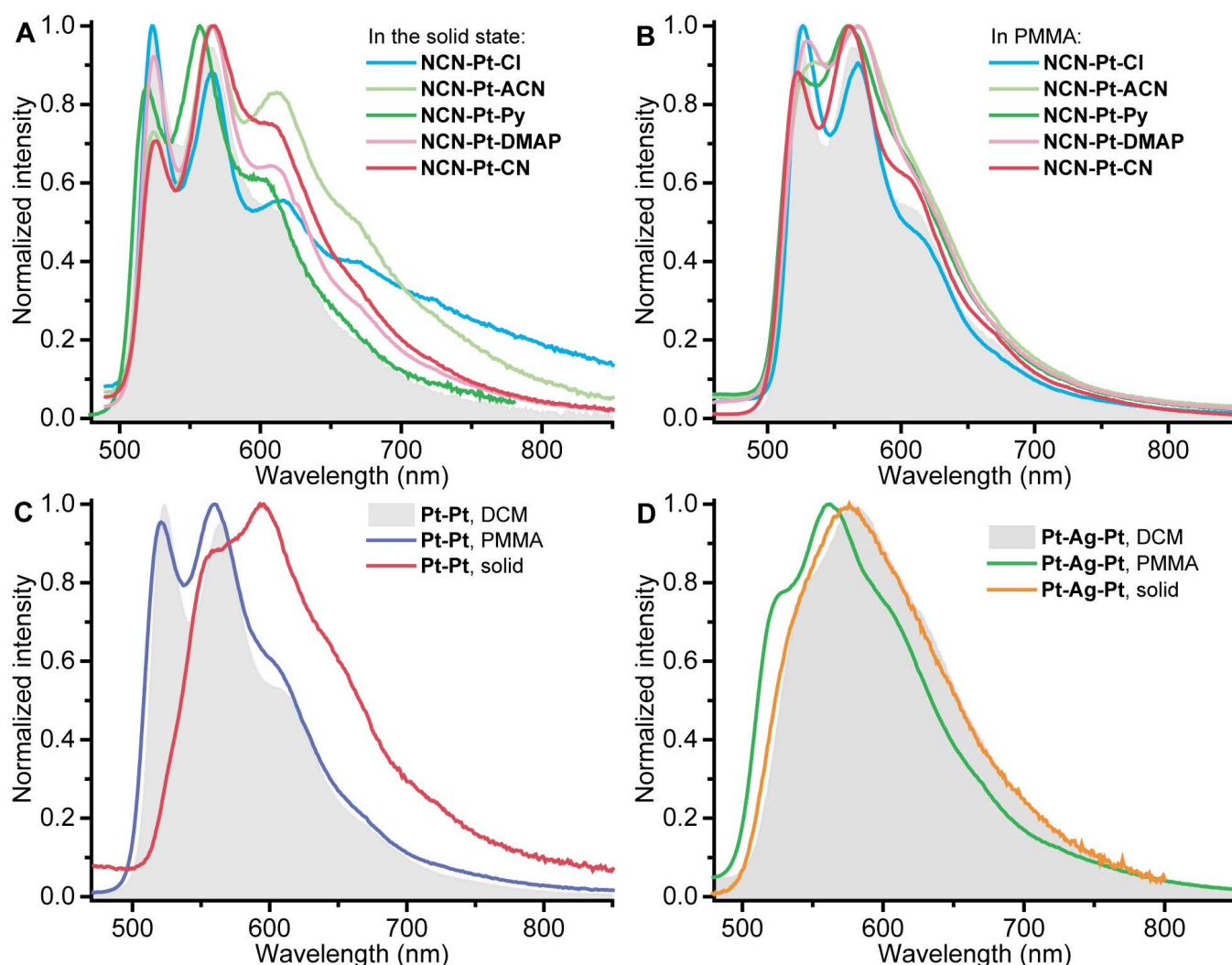


Figure 8. Emission spectra of complexes in PMMA film and in the solid state, $\lambda_{\text{ex}} = 365$ nm, 298 K. Gray spectra—emission of NCN-Pt-ACN (A,B), Pt-Pt (C), Pt-Ag-Pt (D) in DCM, 298 K.

Similarly, the bimetallic Pt-Pt complex retains the nature of its excited state in the PMMA matrix (Figure 8C). In the solid state, however, the emission spectrum demonstrates a redshift of ca. 35 nm. The profile of the solid-state emission spectrum is broadened compared to that observed in solution but still structured with vibration progression of ca. 1300 cm^{-1} . Therefore, the nature of the emission excited state remains predominantly intraligand localized on the N⁺C⁻N⁻ fragment, as was also observed for some binuclear platinum complexes with a dominating ^3IL emission character [63]. Nevertheless, we cannot exclude the slight contribution of the MMLCT character, which gives the observed redshift of the emission band.

In the case of the heterometallic Pt-Ag-Pt complex, a slight hypsochromic shift of the emission band is observed in the polymer matrix compared with the DCM solution (Figure 8D). This effect is often observed for the compounds with a charge transfer nature of the emissive excited state due to an increase in the rigidity of the environment [64,65]. In the solid state, however, there is practically no change in the position and profile of the phosphorescence spectrum, which indicates that the same excited state is retained both in the crystal phase and in solution with negligible influence of any packing effects.

The quantum yields of all the complexes studied grow significantly when incorporated into a polymer matrix. For instance, the quantum yields of NCN-Pt-L complexes in solution range from 0.1 to 3.6 %, whereas in PMMA the values vary from 11 to 15 %. Together with emission efficiency, the lifetime of the excited state increases significantly from 0.1–2.2 μs in

solution to 5.4–15.5 μs in PMMA. **Pt-Pt** and **Pt-Ag-Pt** also display higher lifetimes (11.5 and 22.2 μs) and quantum yields (14 and 22%) in PMMA. The increase in the quantum yield and lifetime values can be attributed to the suppression of nonradiative relaxation channels caused by restricted vibrational/rotational relaxation in the rigid polymer matrix [66].

3. Materials and Methods

3.1. Synthesis of the Ligand and Complexes

General comments. Phenanthrene-9,10-dione, isophthalaldehyde, aniline hydrochloride, 4-(pyridin-2-yl)benzaldehyde, potassium tetrachloroplatinate, dimethylaminopyridine, and 2,6-dimethylphenylisocyanide were purchased from Sigma-Aldrich (Merck, Munich, Germany) and used as received. The ^1H , ^1H - ^1H COSY, and ^{195}Pt NMR spectra in solution were recorded on a Bruker Avance 400 spectrometer (Bruker, Germany) with chemical shifts referenced to residual solvent resonances. Positive ion mode electrospray ionization mass spectra (ESI⁺) were recorded with a maXis II ESI-QTOF instrument (Bruker, Germany). The C, H, and N elemental analysis was carried out by using vario MICRO cube CHNS-analyzer (Elementar, Germany).

Synthesis of 1,3-bis(1-phenyl-1H-phenanthro[9,10-d]imidazol-2-yl)benzene (**NC(H)N**). Phenanthrene-9,10-dione (500 mg, 2.40 mmol), aniline hydrochloride (775 mg, 5.98 mmol), isophthalaldehyde (161 mg, 1.20 mmol), and ammonium acetate (924 mg, 12 mmol) were suspended in acetic acid (13 mL) in a round bottom flask using an ultrasonic bath. Then, with constant stirring, the reaction mixture was heated to 70 °C in an oil bath for 3 h. After the reaction mixture was cooled to room temperature, white precipitate was separated using centrifugation, washed with small amounts of methanol (5 \times 5 mL) and diethyl ether (3 \times 10 mL), and dried under vacuum. Yield of white amorphous precipitate: 750 mg, 1.13 mmol, 94%. Crystals suitable for XRD were obtained by slow diffusion of diethyl ether into the solution of **NC(H)N** in dichloromethane. ^1H NMR (400 MHz, DMSO, 298 K) δ 8.95 (d, $^3J_{\text{H,H}} = 8.3$ Hz, 2H), 8.90 (d, $^3J_{\text{H,H}} = 8.4$ Hz, 2H), 8.72 (dd, $^3J_{\text{H,H}} = 8.0$, $^4J_{\text{H,H}} = 1.1$ Hz, 2H), 8.09 (t, $^4J_{\text{H,H}} = 1.6$ Hz, 1H), 7.82 (t, $^3J_{\text{H,H}} = 7.5$ Hz, 2H), 7.76–7.67 (m, 12H), 7.58 (td, $^3J_{\text{H,H}} = 7.7$, $^4J_{\text{H,H}} = 1.1$ Hz, 2H), 7.47 (dd, $^3J_{\text{H,H}} = 7.8$, $^4J_{\text{H,H}} = 1.7$ Hz, 2H), 7.35 (td, $^3J_{\text{H,H}} = 7.7$, $^4J_{\text{H,H}} = 0.7$ Hz, 2H), 7.28 (t, $^3J_{\text{H,H}} = 7.9$ Hz, 1H), 7.09 (d, $^3J_{\text{H,H}} = 7.6$ Hz, 2H) ppm. Anal. Calcd for $\text{C}_{48}\text{H}_{30}\text{N}_4 + 1/3 \text{H}_2\text{O}$ (%): C, 86.20; H, 4.62; N, 8.38; found: C, 86.06; H, 4.58; N, 8.43. ESI-HRMS (m/z): $[\text{M}+\text{H}]^+$ 663.2539 (calcd. 663.2549).

Synthesis of the Complexes.

NCN-Pt-Cl. **NC(H)N** (200 mg, 0.30 mmol) in acetic acid (15 mL) was suspended with potassium tetrachloroplatinate (153.2 mg, 0.33 mmol) in an ultrasonic bath in a Schlenk flask. The mixture was then deoxygenated by purging with argon for 30 min. The mixture was refluxed at 118 °C in an oil bath under argon for 4 days or 2 weeks. After cooling the reaction mixture to room temperature, the precipitate formed was separated by centrifugation and washed with water 2 \times 5 mL, methanol 2 \times 5 mL, and diethyl ether 2 \times 5 mL, and dried under vacuum. After that, the product was recrystallized by slow diffusion of diethyl ether to dichloromethane solution through the gas phase. Crystals suitable for XRD were obtained in this way. Yield of yellow–green crystalline product: 65 mg, 22% (4 days) and 222 mg, 75% (2 weeks). ^1H NMR (400 MHz, DMSO- d_6 , 298 K) δ 10.38 (d, $^3J_{\text{H,H}} = 8.1$ Hz, 2H), 8.98 (d, $^3J_{\text{H,H}} = 8.5$ Hz, 2H), 8.90 (d, $^3J_{\text{H,H}} = 8.4$ Hz, 2H), 8.05 (d, $^3J_{\text{H,H}} = 7.0$ Hz, 4H), 7.98–7.88 (m, 8H), 7.81 (t, $^3J_{\text{H,H}} = 7.6$ Hz, 2H), 7.66 (t, $^3J_{\text{H,H}} = 7.7$ Hz, 2H), 7.40 (t, $^3J_{\text{H,H}} = 7.7$ Hz, 2H), 7.14 (d, $^3J_{\text{H,H}} = 8.3$ Hz, 2H), 6.72 (t, $^3J_{\text{H,H}} = 7.9$ Hz, 1H), 5.84 (d, $^3J_{\text{H,H}} = 7.9$ Hz, 2H) ppm. Anal. Calcd for $\text{C}_{48}\text{H}_{29}\text{N}_4\text{PtCl} + 1/2 \text{H}_2\text{O}$ (%): C, 63.96; H, 3.36; N, 6.22; found: C, 63.93; H, 3.50; N, 6.16. ESI-HRMS (m/z): $[\text{M}-\text{Cl}]^+$ 856.2044 (calcd. 856.2044).

NCN-Pt-ACN. **NCN-Pt-Cl** (50 mg, 0.056 mmol) and silver hexafluorophosphate (21.3 mg, 0.084 mmol) were suspended in acetonitrile (20 mL) using ultrasonic bath. The reaction mixture was then stirred for 1.5 h at room temperature in the dark. After, the reaction mixture was filtered through Celites and silica gel using dichloromethane as an eluent. The product was obtained as orange crystals after recrystallization from dichloromethane by slow diffusion of diethyl ether through the gas phase. Yield: 50 mg, 0.048 mmol, 86%.

^1H NMR (400 MHz, CD_2Cl_2 , 298 K) δ 9.43 (d, $^3J_{\text{H,H}} = 7.9$ Hz, 2H), 8.92–8.78 (m, 4H), 8.01 (t, $^3J_{\text{H,H}} = 7.4$ Hz, 2H), 7.98–7.84 (m, 8H), 7.74 (d, $^3J_{\text{H,H}} = 7.6$ Hz, 4H), 7.70 (t, $^3J_{\text{H,H}} = 7.8$ Hz, 2H), 7.41 (t, $J = ^3J_{\text{H,H}} = \text{Hz}$, 2H), 7.23 (d, $^3J_{\text{H,H}} = 8.2$ Hz, 2H), 6.71 (t, $^3J_{\text{H,H}} = 7.9$ Hz, 1H), 6.00 (d, $^3J_{\text{H,H}} = 7.9$ Hz, 2H), 1.99 (s, 3H) ppm. Anal. Calcd for $\text{C}_{50}\text{H}_{32}\text{N}_5\text{PtPF}_6 + \text{H}_2\text{O}(\%)$: C, 56.61; H, 3.23; N, 6.60; found: C, 56.49; H, 3.19; N, 6.55. ESI-HRMS (m/z): $[\text{M-PF}_6\text{-ACN}]^+$ 856.2044 (calcd. 856.2044), $[\text{M-PF}_6]^+$ 897.2315 (calcd. 897.2309).

NCN-Pt-Py. **NCN-Pt-Cl** (50 mg, 0.056 mmol) and silver hexafluorophosphate (21.3 mg, 0.084 mmol) were suspended in dichloromethane (12 mL) and pyridine (4 mL) mixture using ultrasonic bath. The reaction mixture was then stirred for 1.5 h at room temperature in the dark. The reaction mixture was filtered through Celites and silica gel using dichloromethane as an eluent. The product was obtained as yellow crystals after recrystallization from dichloromethane/heptane mixture by slow evaporation of dichloromethane at 4 °C. Yield: 42 mg, 0.039 mmol, 70%. ^1H NMR (400 MHz, CD_2Cl_2 , 298 K) δ 8.83 (d, $^3J_{\text{H,H}} = 4.9$ Hz, 1H), 8.77 (d, $^3J_{\text{H,H}} = 8.3$ Hz, 1H), 8.65 (d, $^3J_{\text{H,H}} = 8.4$ Hz, 1H), 7.99–7.94 (m, 1H), 7.91 (t, $^3J_{\text{H,H}} = 7.5$ Hz, 3H), 7.84 (d, $^3J_{\text{H,H}} = 7.3$ Hz, 2H), 7.68 (td, $^3J_{\text{H,H}} = 7.7$, 0.8 Hz, 1H), 7.56 (d, $^3J_{\text{H,H}} = 8.0$ Hz, 1H), 7.47–7.39 (m, 2H), 7.35 (dd, $^3J_{\text{H,H}} = 7.5$, 6.4 Hz, 1H), 7.27 (d, $^3J_{\text{H,H}} = 8.1$ Hz, 1H), 6.77–6.72 (m, 1H), 6.05 (d, $^3J_{\text{H,H}} = 7.9$ Hz, 1H) ppm. ESI-MS (m/z): $[\text{M-PF}_6\text{-ACN}]^+$ 856.2022 (calcd. 856.2044), $[\text{M-PF}_6]^+$ 935.2439 (calcd. 935.2466). Anal. Calcd for $\text{C}_{53}\text{H}_{34}\text{N}_5\text{PtPF}_6 + \text{H}_2\text{O}(\%)$: C, 57.93; H, 3.30; N, 6.37; found: C, 57.91; H, 3.19; N, 6.02.

NCN-Pt-DMAP. **NCN-Pt-Cl** (35 mg, 0.039 mmol) was suspended in dichloromethane (7 mL) with dimethylaminopyridine (DMAP) (5.5 mg, 0.045 mmol) and silver hexafluorophosphate (11.4 mg, 0.045 mmol) using an ultrasonic bath for an hour. Then, the reaction mixture was continuously stirred for 4 days in the dark at room temperature. The reaction mixture was filtered through Celites and silica gel using dichloromethane as eluent. The product was obtained as yellow crystals after recrystallization by slow diffusion of diethyl ether in the dichloromethane solution through the gas phase. Yield: 26 mg, 0.023 mmol, 59%. ^1H NMR (400 MHz, CD_2Cl_2 , 298 K) δ 8.78 (d, $^3J_{\text{H,H}} = 8.4$ Hz, 2H), 8.66 (d, $^3J_{\text{H,H}} = 8.3$ Hz, 2H), 8.19 (d, $^3J_{\text{H,H}} = 7.1$ Hz, 2H), 7.95 (t, $^3J_{\text{H,H}} = 7.3$ Hz, 2H), 7.92–7.81 (m, 10H), 7.68 (td, $^3J_{\text{H,H}} = 7.7$, $^4J_{\text{H,H}} = 1.0$ Hz, 2H), 7.49 (t, $^3J_{\text{H,H}} = 7.7$, $^4J_{\text{H,H}} = 1.2$ Hz, 2H), 7.40 (t, $^3J_{\text{H,H}} = 7.3$ Hz, 2H), 7.26 (d, $^3J_{\text{H,H}} = 8.2$ Hz, 2H), 6.88 (t, $^3J_{\text{H,H}} = 7.8$ Hz, 2H), 6.71 (t, $^3J_{\text{H,H}} = 7.9$ Hz, 1H), 6.39 (d, $^3J_{\text{H,H}} = 7.1$ Hz, 2H), 6.02 (d, $^3J_{\text{H,H}} = 7.9$ Hz, 2H), 3.09 (s, 6H) ppm. ESI-HRMS (m/z): $[\text{M-PF}_6\text{-DMAP}]^+$ 856.2041 (calcd. 856.2044), $[\text{M-PF}_6]^+$ 978.2875 (calcd. 978.2888). Anal. Calcd for $\text{C}_{55}\text{H}_{39}\text{N}_6\text{PtPF}_6(\%)$: C, 58.77; H, 3.50; N, 7.48; found: C, 58.40; H, 3.54; N, 6.80.

NCN-Pt-CN. **NCN-Pt-Cl** (40 mg, 0.045 mmol) was suspended in dichloromethane solution (10 mL) with silver hexafluorophosphate (10 mg, 0.052 mmol) and 2,6-dimethylphenylisocyanide (10 mg, 0.08 mmol) in an ultrasonic bath for 2 h with heating up to 48 °C. The reaction mixture was dried by distilling off the solvent under reduced pressure without heating. The precipitate was dissolved in acetone. After filtration through Celites, the filtrate was passed through silica gel, and the product was recrystallized by slow diffusion of diethyl ether in dichloromethane solution. Yield of yellow prismatic crystals: 19 mg, 0.017 mmol, 37%. ^1H NMR (400 MHz, acetone- d_6 , 298 K) δ 9.80 (d, $^3J_{\text{H,H}} = 7.5$ Hz, 2H), 9.05 (m, 4H), 8.18 (t, $^3J_{\text{H,H}} = 8.1$ Hz, 2H), 8.15 (d, $^3J_{\text{H,H}} = 7.9$ Hz, 4H), 8.07–8.00 (m, 6H), 7.89 (t, $^3J_{\text{H,H}} = 7.6$ Hz, 2H), 7.76 (t, $^3J_{\text{H,H}} = 7.2$ Hz, 2H), 7.49 (t, $^3J_{\text{H,H}} = 7.9$ Hz, 2H), 7.33 (d, $^3J_{\text{H,H}} = 8.4$ Hz, 2H), 7.18 (t, $^3J_{\text{H,H}} = 7.8$ Hz, 1H), 6.96 (d, $^3J_{\text{H,H}} = 7.5$ Hz, 2H), 6.94 (t, $^3J_{\text{H,H}} = 7.8$ Hz, 1H), 6.22 (d, $^3J_{\text{H,H}} = 7.9$ Hz, 2H), 1.57 (s, 6H) ppm. ESI-HRMS (m/z): $[\text{M-PF}_6]^+$ 1118.3522 (calcd. 1118.3515).

Pt-Pt. **NCN-Pt-Cl** (40 mg, 0.045 mmol), silver hexafluorophosphate (6.4 mg, 0.02 mmol) were suspended in dichloromethane (2.5 mL), ethyl acetate (2.5 mL), and acetic acid (5.4 μL) using ultrasonic bath within 1 h with heating up to 48 °C. The solvents were evaporated under reduced pressure. The precipitate was dissolved in acetone. After filtration through Celites, the filtrate was recrystallized from ethyl acetate. Yield of

yellow crystals: 24 mg, 0.012 mmol, 55%. ^1H NMR (400 MHz, CD_2Cl_2 , 298 K) δ 9.34 (dd, $^3J_{\text{H,H}} = 8.0$, $^4J_{\text{H,H}} = 1.0$ Hz, 1H), 8.64 (d, $^3J_{\text{H,H}} = 8.3$ Hz, 1H), 8.30 (d, $^3J_{\text{H,H}} = 8.2$ Hz, 1H), 7.75 (t, $^3J_{\text{H,H}} = 7.7$ Hz, 1H), 7.67 (td, $^3J_{\text{H,H}} = 7.6$, $^4J_{\text{H,H}} = 0.7$ Hz, 1H), 7.58 (td, $^3J_{\text{H,H}} = 7.8$, $^4J_{\text{H,H}} = 1.2$ Hz, 1H), 7.40 (td, $^3J_{\text{H,H}} = 7.8$, $^4J_{\text{H,H}} = 1.1$ Hz, 1H), 7.34 (td, $^3J_{\text{H,H}} = 7.6$, $^4J_{\text{H,H}} = 0.6$ Hz, 1H), 7.24 (td, $^3J_{\text{H,H}} = 7.6$, $^4J_{\text{H,H}} = 1.1$ Hz, 1H), 7.20–7.14 (m, 2H), 6.77 (d, $^3J_{\text{H,H}} = 8.4$ Hz, 2H), 6.47 (t, $^3J_{\text{H,H}} = 7.8$ Hz, 1H), 5.52 (d, $^3J_{\text{H,H}} = 7.8$ Hz, 1H), 2.04 (s, 1H) ppm. Anal. Calcd for $\text{C}_{98}\text{H}_{61}\text{N}_8\text{O}_2\text{Pt}_2\text{PF}_6$ (%): C, 61.38; H, 3.21; N, 5.84; found: C, 59.21; H, 3.37; N, 6.39. ESI-HRMS (m/z): $[\text{1/2}(\text{M}-\text{CH}_3\text{COO}-\text{PF}_6)]^+$ 856.2046 (calcd. 856.2044), $[\text{M}-\text{CH}_3\text{COO}-\text{PF}_6+\text{Cl}]^+$ 1748.3767 (calcd. 1748.3785).

Pt-Ag-Pt. NCN-Pt-Cl (40 mg, 0.045 mmol), silver hexafluorophosphate (23 mg, 0.09 mmol), and 2,6-dimethylphenylisocyanide (13 mg, 0.10 mmol) were suspended in dichloromethane (10 mL) using ultrasonic bath for 2 h with heating up to 48 °C. The solvent was evaporated under reduced pressure. The crude product was dissolved in dichloromethane and filtered through Celites. The filtrate was recrystallized by slow diffusion of diethyl ether to the solution. Yield of yellow crystals: 39 mg, 0.014 mmol, 63%. ^1H NMR (400 MHz, acetone- d_6 , 298 K) δ 10.47 (d, $^3J_{\text{H,H}} = 7.9$ Hz, 2H), 9.39 (d, $^3J_{\text{H,H}} = 8.5$ Hz, 2H), 9.12 (d, $^3J_{\text{H,H}} = 8.5$ Hz, 2H), 8.95 (d, $^3J_{\text{H,H}} = 8.3$ Hz, 2H), 8.80 (d, $^3J_{\text{H,H}} = 8.3$ Hz, 2H), 8.23 (t, $^3J_{\text{H,H}} = 7.9$ Hz, 2H), 8.11 (m, 6H), 8.07 (d, $^3J_{\text{H,H}} = 7.7$ Hz, 2H), 7.98–7.87 (m, 6H), 7.80–7.74 (m, 4H), 7.49 (t, $^3J_{\text{H,H}} = 7.5$ Hz, 2H), 7.46–7.40 (m, 4H), 7.28–7.21 (m, 4H), 7.13–6.97 (m, 8H), 6.89 (t, $^3J_{\text{H,H}} = 8.0$ Hz, 2H), 6.85–6.76 (m, 6H), 6.64 (d, $^3J_{\text{H,H}} = 8.2$ Hz, 2H), 6.57–6.53 (m, 6H), 5.69 (t, $^3J_{\text{H,H}} = 7.5$ Hz, 2H), 5.52 (d, $^3J_{\text{H,H}} = 7.4$ Hz, 2H), 2.02 (s, 12H), 1.38 (s, 12H) ppm. ^{195}Pt NMR (86 MHz, acetone- d_6 , 298 K) δ -3978.05 (s) ppm. Anal. Calcd for $\text{C}_{132}\text{H}_{94}\text{N}_{12}\text{AgPt}_2\text{P}_3\text{F}_{18} + 3\text{CH}_2\text{Cl}_2$ (%): C, 53.41; H, 3.32; N, 5.54; found: C, 53.12; H, 3.63; N, 5.67. ESI-HRMS (m/z): $[\text{1/2}(\text{M}-3\text{PF}_6-\text{Ag})]^+$ 1118.3513 (calcd. 1118.3515).

3.2. X-ray Diffraction Analysis

The crystals of **NCN-Pt-Cl** and **Pt-Ag-Pt** suitable for XRD analysis, was grown in CH_2Cl_2 by slow diffusion of diethyl ether at RT. The crystals of **NCN-Pt-Py** and **NCN-Pt-CN** suitable for XRD analysis, were obtained from CH_2Cl_2 /hexane mixture via slow evaporation of CH_2Cl_2 from the solution at RT. Complex **NCN-Pt-ACN** was crystallized from acetonitrile/diethyl ether mixture by slow diffusion of diethyl ether in acetonitrile at RT. The crystal of **Pt-Pt** was obtained from ethyl acetate due to evaporation of the solvent. The diffraction data of **NCN-Pt-Cl**, **NCN-Pt-Py**, and **NCN-Pt-CN** was collected with an XtaLAB Synergy HyPix diffractometer, and the data for **NCN-Pt-ACN**, **Pt-Pt**, and **Pt-Ag-Pt** was collected with a SuperNova HyPix-3000 diffractometer. All the measurements were carried out using monochromatic $\text{CuK}\alpha$ radiation at a temperature of 100K. Diffraction data were processed in *CrysAlisPro* program [67]. The structure was solved using Olex2 [68] with the SHELXS [69] structure solution program using direct methods and refined using the SHELXL [70] package. The unit cells of **NCN-Pt-Cl**, **NCN-Pt-ACN**, **NCN-Pt-CN**, **Pt-Pt**, and **Pt-Ag-Pt** contain disordered solvent molecules which have been treated as a diffuse contribution to the overall scattering without specific atom positions by solvent mask instrument integrated into Olex2 [71].

Supplementary crystallographic data for this paper have been deposited at Cambridge Crystallographic Data Centre and can be obtained free of charge via www.ccdc.cam.ac.uk/structures/, accessed on 1 May 2023. **NCN-Pt-Cl** (Pna 2_1 ; a = 15.3721(2), b = 17.0053(2), c = 30.0534(3) Å; $\alpha = \beta = \gamma = 90^\circ$; V = 7856.17(16) Å 3 ; Z = 8; R1 = 4.30%; CCDC 2242753). **NCN-Pt-ACN** (C2/c; a = 20.8432(2), b = 29.6127(3), c = 17.6765(2) Å; $\alpha = \gamma = 90$, $\beta = 90.0950(10)^\circ$; V = 10910.3(2) Å 3 ; Z = 8; R1 = 4.38%; CCDC 2242764). **NCN-Pt-Py** (P2 $_1$ /c; a = 22.0458(2), b = 9.63000(10), c = 23.7845(2) Å; $\alpha = \gamma = 90$, $\beta = 105.3730(10)^\circ$; V = 4868.81(8) Å 3 ; Z = 4; R1 = 3.11%; CCDC 2242765). **NCN-Pt-CN** (P2 $_1$ /n; a = 16.9422(2), b = 17.69520(10), c = 18.3812(2) Å; $\alpha = \gamma = 90$, $\beta = 116.589(2)^\circ$; V = 4927.80(11) Å 3 ; Z = 8; R1 = 3.59%; CCDC 2242766). **Pt-Pt** (P-1; a = 17.4175(2), b = 17.4217(3), c = 17.9119(2) Å; $\alpha = 88.0990(10)$, $\beta = 65.5390(10)$, $\gamma = 67.428(2)^\circ$; V = 4516.97(13) Å 3 ; Z = 2; R1 = 5.42%; CCDC 2242769). **Pt-Ag-Pt** P-1; a = 17.4754(3), b = 24.8036(5), c = 28.7013(4) Å;

$\alpha = 71.253(2)$, $\beta = 76.9150(10)$, $\gamma = 88.743(2)^\circ$; $V = 11457.3(4) \text{ \AA}^3$; $Z = 4$; $R1 = 7.09\%$; CCDC 2242797).

3.3. Photophysical Measurements

Photophysical properties in solution were investigated using distilled CH_2Cl_2 . The solutions were deoxygenated by purging of argon for 15–20 min. UV/Vis absorption spectra were recorded with a Shimadzu UV-1800 spectrophotometer at concentrations of ca. $5 \times 10^{-5} \text{ M}$ in 1 cm quartz cuvettes. Emission spectra were measured using an Avantes AvaSpec-2048 \times 64 spectrometer (Avantes, Apeldoorn, Netherlands), emission of solid samples was measured using Avantes reflection probe for powders FCR-7UVIR200-2-45-ME. Excitation spectra in the solid state and in polymeric matrix were recorded on a Fluorolog-3 (JY Horiba Inc., Japan) spectrofluorometer. The emission quantum yields in solution were determined by the comparative method [72] using $\text{Ru}(\text{bpy})_3^+$ in aerated water ($\Phi_r = 0.040$) [73] as the reference (the refractive indices of dichloromethane and water equal to 1.42 and 1.33, respectively). The absolute emission quantum yields in solid state and in PMMA matrix were measured using Avantes Integration sphere (Avantes, Apeldoorn, Netherlands). Emission lifetime measurements were carried out using a device comprised of a Pulse laser TECH-263 Basic (for phosphorescence lifetime, wavelength 355 nm, pulse width 5 ns, repetition frequency 1000 Hz) (Laser Export, Moscow, Russia) or LDH-P-C-405 (for fluorescence lifetime, wavelength 405 nm, pulse width 50 ps, repetition frequency of 10 MHz) (PicoQuant, Berlin, Germany), a Hamamatsu H10682-01 photon counting head (Hamamatsu, Hamamatsu, Japan), a FASTComTec MCS6A1T4 multiple-event time digitizer (FAST ComTec, Oberhaching, Germany) and an Ocean Optics monochromator Monoscan-2000 (interval of wavelengths 1 nm; Ocean Optics, Largo, FL, USA). Mono- and biexponential decay fit of lifetime data was carried out by using the Origin 9.0 and the Jobin Yvon software packages.

3.4. Computational Details

Ground and excited triplet state structures were optimized for studied compounds using density functional theory (DFT). All calculations were performed using the Gaussian-16 software [74]. The MN12SX [75] functional was used due to the best agreement with experimental results. The Stuttgart–Dresden effective core pseudopotential (SDD) [76] was used for all atoms. The non-specific solvation effect of dichloromethane was simulated by the polarizable continuum model (PCM) [77].

The absorption spectra were calculated within TD-DFT methodology with 120–200 excited states for all complexes. The convoluting of absorption spectra in UV–Vis range from calculated oscillator strengths using method [78] modified for Lorentzian with a band broadening of 1500 cm^{-1} . The energies of phosphorescence maxima were obtained as “vertical” transition—energy difference between the optimized triplet state and the singlet form in the geometry of previously optimized first triplet state (as “vertical” transition).

Characterization of the electron density displacement during absorption and emission transitions was established by the construction of NTO (natural transition orbitals) [79] and by calculation of IFCT (interfragment charge transfer) method [80]. The Multiwfn 3.6 software [80] was used for both methods. The changes in electronic density $\Delta\rho$ during the $S_0 \rightarrow S_i$ transitions were calculated as:

$$\Delta\rho(S_0 \rightarrow S_i) = \sum_k |\Psi_{ik}(\text{virt})|^2 - \sum_k |\Psi_{ik}(\text{occ})|^2$$

where $\Psi_{ik}(\text{occ})$ and $\Psi_{ik}(\text{virt})$ are NTO pairs for $S_0 \rightarrow S_i$ transition. In the same way, were calculated electron density transfer of the emission transition $T_1 \rightarrow S_0$.

4. Conclusions

A series of luminescent $[\text{Pt}(\text{N}^{\wedge}\text{C}^{\wedge}\text{N})\text{L}]$ complexes based on a novel 1,3-bis(1-phenyl-1H-phenanthro[9,10-d]imidazol-2-yl)benzene ligand have been synthesized and characterized.

The choice of the bulky cyclometallated pincer ligand dictates the structural peculiarities of the obtained compounds, their chemical behavior and stability in solution, and their photophysical properties. The ancillary ligands (L) strongly affect the molecular structure of the obtained complexes to give a significant distortion of the square planar geometry of the complex, which in turn results in the unusual photophysics of the chloride complex. The use of bidentate acetate allowed for obtaining a binuclear bridging complex with a short metal–metal contact. In addition, due to the lability of the pincer chelate, a heterometallic trinuclear {AgPt₂} complex was obtained with 2,6-dimethylphenylisocyanide in the presence of silver salt. The photophysics of the complexes was studied in detail in a solution of DCM, PMMA matrix, and in the solid state. The compounds exhibit phosphorescence at 450–600 nm with quantum yields up to ca. 20% and lifetimes of the excited state in the microsecond domain. The chloride complex displays dual (fluorescence and phosphorescent) luminescence due to the labile coordination of an N-coordinated functionality that produces a dangling aromatic fragment. The latter gives emission from the singlet excited state together with the phosphorescence originating from the starting complex, which exists in equilibrium with the dissociative form. DFT and TD DFT calculations made a possible detailed assignment of electronic transitions responsible for the absorption and emission of mononuclear compounds.

Supplementary Materials: The following supporting information can be downloaded at: <https://www.mdpi.com/article/10.3390/inorganics11050198/s1>, XRD-analysis: Tables S1–S2, Figure S1, ESI mass spectrometry and NMR spectroscopy data: Figures S2–S14, Photophysical data: Figures S15–S20, Computational results: Tables S3–S12, Figures S21–S24.

Author Contributions: Conceptualization, A.I.S. and S.P.T.; methodology, A.I.S.; validation, S.P.T.; formal analysis, E.E.L., A.I.S., D.O.K.; investigation, E.E.L., A.I.S., D.O.K., A.V.M.; resources, S.P.T., A.I.S.; data curation, A.I.S.; writing—original draft preparation E.E.L., A.I.S., D.O.K. and S.P.T.; writing—review and editing, A.I.S., S.P.T. and V.V.P.; visualization, A.I.S. and D.O.K.; supervision, A.I.S. and S.P.T.; project administration, A.I.S. and S.P.T.; funding acquisition, A.I.S. All authors have read and agreed to the published version of the manuscript.

Funding: This research was funded by the Council for Grants of the President of the Russian Federation No. MK-1953.2021.1.3.

Data Availability Statement: Data are contained within the article and Supplementary Material.

Acknowledgments: This study was carried out using the equipment of the Research Park of St. Petersburg State University: Computing Centre, Centers for Optical and Laser Materials Research, for Magnetic Resonance, for Chemical Analysis and Materials Research, and for X-ray Diffraction Studies.

Conflicts of Interest: The authors declare no conflict of interest.

References

1. Li, K.; Ming Tong, G.S.; Wan, Q.; Cheng, G.; Tong, W.-Y.Y.; Ang, W.-H.H.; Kwong, W.-L.L.; Che, C.-M.M. Highly phosphorescent platinum(II) emitters: Photophysics, materials and biological applications. *Chem. Sci.* **2016**, *7*, 1653–1673. [[CrossRef](#)]
2. Huo, S.; Carroll, J.; Vezzu, D.A.K. Design, Synthesis, and Applications of Highly Phosphorescent Cyclometalated Platinum Complexes. *Asian J. Org. Chem.* **2015**, *4*, 1210–1245. [[CrossRef](#)]
3. Kalinowski, J.; Fattori, V.; Cocchi, M.; Williams, J.A.G. Light-emitting devices based on organometallic platinum complexes as emitters. *Coord. Chem. Rev.* **2011**, *255*, 2401–2425. [[CrossRef](#)]
4. Dorazco-González, A. Use of Pincer Compounds as Metal-Based Receptors for Chemosensing of Relevant Analytes. In *Pincer Compounds*; Elsevier: Amsterdam, The Netherlands, 2018; pp. 587–597.
5. Yeung, M.C.-L.; Yam, V.W.-W. Luminescent cation sensors: From host–guest chemistry, supramolecular chemistry to reaction-based mechanisms. *Chem. Soc. Rev.* **2015**, *44*, 4192–4202. [[CrossRef](#)] [[PubMed](#)]
6. Jiang, X.; Zhu, N.; Zhao, D.; Ma, Y. New cyclometalated transition-metal based photosensitizers for singlet oxygen generation and photodynamic therapy. *Sci. China Chem.* **2016**, *59*, 40–52. [[CrossRef](#)]
7. Lo, K.K.-W.; Choi, A.W.-T.; Law, W.H.-T. Applications of luminescent inorganic and organometallic transition metal complexes as biomolecular and cellular probes. *Dalt. Trans.* **2012**, *41*, 6021. [[CrossRef](#)] [[PubMed](#)]

8. Mauro, M.; Aliprandi, A.; Septiadi, D.; Kehr, N.S.; De Cola, L. When self-assembly meets biology: Luminescent platinum complexes for imaging applications. *Chem. Soc. Rev.* **2014**, *43*, 4144–4166. [[CrossRef](#)] [[PubMed](#)]
9. Qiu, K.; Chen, Y.; Rees, T.W.; Ji, L.; Chao, H. Organelle-targeting metal complexes: From molecular design to bio-applications. *Coord. Chem. Rev.* **2019**, *378*, 66–86. [[CrossRef](#)]
10. Baggaley, E.; Weinstein, J.A.; Williams, J.A.G. Lighting the way to see inside the live cell with luminescent transition metal complexes. *Coord. Chem. Rev.* **2012**, *256*, 1762–1785. [[CrossRef](#)]
11. Arrowsmith, R.L.; Pascu, S.I.; Smugowski, H. New developments in the biomedical chemistry of metal complexes: From small molecules to nanotheranostic design. In *Organometallic Chemistry*; RSC Publishing: Cambridge, UK, 2012; Volume 38, pp. 1–35. ISBN 9781849733762.
12. Tunik, S.P.; Chelushkin, P.S.; Shakirova, J.R.; Kritchenkov, I.; Baigildin, V.A. Phosphorescent NIR emitters for biomedicine: Applications, advances and challenges. *Dalt. Trans.* **2021**. [[CrossRef](#)]
13. Aliprandi, A.; Genovese, D.; Mauro, M.; De Cola, L. Recent Advances in Phosphorescent Pt(II) Complexes Featuring Metallophilic Interactions: Properties and Applications. *Chem. Lett.* **2015**, *44*, 1152–1169. [[CrossRef](#)]
14. Solomatina, A.I.; Galenko, E.E.; Kozina, D.O.; Kalinichev, A.A.; Baigildin, V.A.; Prudovskaya, N.A.; Shakirova, J.R.; Khlebnikov, A.F.; Porsev, V.V.; Evarestov, R.A.; et al. Nonsymmetric [Pt(C[∞]N[∞]N[∞]C[∞])] Complexes: Aggregation-Induced Emission in the Solid State and in Nanoparticles Tuned by Ligand Structure. *Chem. A Eur. J.* **2022**, *28*. [[CrossRef](#)] [[PubMed](#)]
15. Gabr, M.T.; Pigge, F.C. Platinum(II) Complexes with Sterically Expansive Tetraarylethylene Ligands as Probes for Mismatched DNA. *Inorg. Chem.* **2018**, *57*, 12641–12649. [[CrossRef](#)] [[PubMed](#)]
16. Chan, K.; Chung, C.Y.-S.; Yam, V.W.-W. Parallel folding topology-selective label-free detection and monitoring of conformational and topological changes of different G-quadruplex DNAs by emission spectral changes via FRET of mPPE-Ala-Pt(II) complex ensemble. *Chem. Sci.* **2016**, *7*, 2842–2855. [[CrossRef](#)] [[PubMed](#)]
17. Williams, J.A.G.; Beeby, A.; Davies, E.S.; Weinstein, J.A.; Wilson, C. An Alternative Route to Highly Luminescent Platinum(II) Complexes: Cyclometalation with N[∞]C[∞]N[∞]-Coordinating Dipyriddybenzene Ligands. *Inorg. Chem.* **2003**, *42*, 8609–8611. [[CrossRef](#)]
18. Puttock, E.V.; Walden, M.T.; Williams, J.A.G. The luminescence properties of multinuclear platinum complexes. *Coord. Chem. Rev.* **2018**, *367*, 127–162. [[CrossRef](#)]
19. Katlenok, E.A.; Haukka, M.; Levin, O.V.; Frontera, A.; Kukushkin, V.Y. Supramolecular Assembly of Metal Complexes by (Aryl)I[∞]⋯d[Pt II] Halogen Bonds. *Chem. A Eur. J.* **2020**, *26*, 7692–7701. [[CrossRef](#)]
20. Berenguer, J.R.; Lalinde, E.; Moreno, M.T. Luminescent cyclometalated-pentafluorophenyl PtII, PtIV and heteropolynuclear complexes. *Coord. Chem. Rev.* **2018**, *366*, 69–90. [[CrossRef](#)]
21. Baya, M.; Belío, Ú.; Forniés, J.; Martín, A.; Perálvarez, M.; Sicilia, V. Neutral benzoquinolate cyclometalated platinum(II) complexes as precursors in the preparation of luminescent Pt–Ag complexes. *Inorganica Chim. Acta* **2015**, *424*, 136–149. [[CrossRef](#)]
22. Zhang, X.-P.; Chang, Y.Y.; Liu, J.; Yang, X.-L.; Huang, W.; Li, Y.; Li, C.-H.; Muller, G.; You, X.-Z. Potential Switchable Circularly Polarized Luminescence from Chiral Cyclometalated Platinum(II) Complexes. *Inorg. Chem.* **2015**, *54*, 143–152. [[CrossRef](#)]
23. Berenguer, J.R.; Lalinde, E.; Teresa Moreno, M. An overview of the chemistry of homo and heteropolynuclear platinum complexes containing bridging acetylide (μ -C \equiv CR) ligands. *Coord. Chem. Rev.* **2010**, *254*, 832–875. [[CrossRef](#)]
24. Williams, J.A.G. Photochemistry and Photophysics of Coordination Compounds: Platinum. In *Photochemistry and Photophysics of Coordination Compounds II*; Balzani, V., Campagna, S., Eds.; Topics in Current Chemistry; Springer: Berlin/Heidelberg, Germany, 2007; Volume 281, pp. 205–268. ISBN 978-3-540-73348-5, 978-3-540-73349-2.
25. Williams, J.A.G. The coordination chemistry of dipyriddybenzene: N-deficient terpyridine or panacea for brightly luminescent metal complexes? *Chem. Soc. Rev.* **2009**, *38*, 1783–1801. [[CrossRef](#)] [[PubMed](#)]
26. Tong, G.S.-M.; Che, C.-M. Emissive or nonemissive? A theoretical analysis of the phosphorescence efficiencies of cyclometalated platinum(II) complexes. *Chem. A Eur. J.* **2009**, *15*, 7225–7237. [[CrossRef](#)]
27. Wang, X.; Yang, H.; Wen, Y.; Wang, L.; Li, J.; Zhang, J. Comprehension of the Effect of a Hydroxyl Group in Ancillary Ligand on Phosphorescent Property for Heteroleptic Ir(III) Complexes: A Computational Study Using Quantitative Prediction. *Inorg. Chem.* **2017**, *56*, 8986–8995. [[CrossRef](#)]
28. Sajoto, T.; Djurovich, P.I.; Tamayo, A.B.; Oxgaard, J.; Goddard, W.A.; Thompson, M.E. Temperature Dependence of Blue Phosphorescent Cyclometalated Ir(III) Complexes. *J. Am. Chem. Soc.* **2009**, *131*, 9813–9822. [[CrossRef](#)]
29. Wang, Z.; Turner, E.; Mahoney, V.; Madakuni, S.; Groy, T.; Li, J. Facile Synthesis and Characterization of Phosphorescent Pt(N[∞]C[∞]N[∞])X Complexes. *Inorg. Chem.* **2010**, *49*, 11276–11286. [[CrossRef](#)]
30. Cárdenas, D.J.; Echavarren, A.M.; Ramírez de Arellano, M.C. Divergent Behavior of Palladium(II) and Platinum(II) in the Metalation of 1,3-Di(2-pyridyl)benzene. *Organometallics* **1999**, *18*, 3337–3341. [[CrossRef](#)]
31. Farley, S.J.; Rochester, D.L.; Thompson, A.L.; Howard, J.A.K.; Williams, J.A.G. Controlling Emission Energy, Self-Quenching, and Excimer Formation in Highly Luminescent N[∞]C[∞]N[∞]-Coordinated Platinum(II) Complexes. *Inorg. Chem.* **2005**, *44*, 9690–9703. [[CrossRef](#)]
32. Tarran, W.A.; Freeman, G.R.; Murphy, L.; Benham, A.M.; Katakay, R.; Williams, J.A.G. Platinum(II) complexes of N[∞]C[∞]N[∞]-coordinating 1,3-bis(2-pyridyl)benzene ligands: Thiolate coligands lead to strong red luminescence from charge-transfer states. *Inorg. Chem.* **2014**, *53*, 5738–5749. [[CrossRef](#)]
33. Haque, A.; Xu, L.; Al-Balushi, R.A.; Al-Suti, M.K.; Ilmi, R.; Guo, Z.; Khan, M.S.; Wong, W.-Y.; Raithby, P.R. Cyclometalated tridentate platinum(II) arylacetylide complexes: Old wine in new bottles. *Chem. Soc. Rev.* **2019**, *48*, 5547–5563. [[CrossRef](#)]

34. Dorazco-Gonzalez, A. Chemosensing of Chloride Based on a Luminescent Platinum(II) NCN Pincer Complex in Aqueous Media. *Organometallics* **2014**, *33*, 868–875. [[CrossRef](#)]
35. Tam, A.Y.-Y.; Tsang, D.P.-K.; Chan, M.-Y.; Zhu, N.; Yam, V.W.-W. A luminescent cyclometalated platinum(II) complex and its green organic light emitting device with high device performance. *Chem. Commun.* **2011**, *47*, 3383. [[CrossRef](#)] [[PubMed](#)]
36. Lam, E.S.-H.; Tsang, D.P.-K.; Lam, W.H.; Tam, A.Y.-Y.; Chan, M.-Y.; Wong, W.-T.; Yam, V.W.-W. Luminescent Platinum(II) Complexes of 1,3-Bis(N -alkylbenzimidazol- 2'-yl)benzene-Type Ligands with Potential Applications in Efficient Organic Light-Emitting Diodes. *Chem. A Eur. J.* **2013**, *19*, 6385–6397. [[CrossRef](#)]
37. Lam, E.S.-H.; Tam, A.Y.-Y.; Chan, M.-Y.; Yam, V.W.-W. A New Class of Luminescent Platinum(II) Complexes of 1,3-Bis(N -alkylbenzimidazol-2'-yl)benzene-Type Ligands and Their Application Studies in the Fabrication of Solution-Processable Organic Light-Emitting Devices. *Isr. J. Chem.* **2014**, *54*, 986–992. [[CrossRef](#)]
38. Han, J.; Wang, Y.; Wang, J.; Wu, C.; Zhang, X.; Yin, X. Amplification of circularly polarized luminescence from chiral cyclometalated platinum(II) complexes by the formation of excimer. *J. Organomet. Chem.* **2022**, *973–974*, 122394. [[CrossRef](#)]
39. Chan, M.H.-Y.; Wong, H.-L.; Yam, V.W.-W. Synthesis and Photochromic Studies of Dithienylethene-Containing Cyclometalated Alkynylplatinum(II) 1,3-Bis(N -alkylbenzimidazol-2'-yl)benzene Complexes. *Inorg. Chem.* **2016**, *55*, 5570–5577. [[CrossRef](#)] [[PubMed](#)]
40. Sun, J.; Yuan, B.; Hou, X.; Yan, C.; Sun, X.; Xie, Z.; Shao, X.; Zhou, S. Broadband optical limiting of a novel twisted tetrathiafulvalene incorporated donor–acceptor material and its Ormosil gel glasses. *J. Mater. Chem. C* **2018**, *6*, 8495–8501. [[CrossRef](#)]
41. Qiu, Y.; Feng, Y.; Zhao, Q.; Wang, H.; Guo, Y.; Qiu, D. White light emission from a green cyclometalated platinum(II) terpyridylphenylacetylde upon titration with Zn(II) and Eu(III). *Dalt. Trans.* **2020**, *49*, 11163–11169. [[CrossRef](#)]
42. Kong, F.K.-W.; Tang, M.-C.; Wong, Y.-C.; Chan, M.-Y.; Yam, V.W.-W. Design Strategy for High-Performance Dendritic Carbazole-Containing Alkynylplatinum(II) Complexes and Their Application in Solution-Processable Organic Light-Emitting Devices. *J. Am. Chem. Soc.* **2016**, *138*, 6281–6291. [[CrossRef](#)]
43. Marqués-López, E.; Herrera, R.P. Essential Multicomponent Reactions I. In *Multicomponent Reactions*; John Wiley & Sons, Inc: Hoboken, NJ, USA, 2015; pp. 382–415.
44. Dias, G.G.; Paz, E.R.S.; Nunes, M.P.; Carvalho, R.L.; Rodrigues, M.O.; Rodembusch, F.S.; Silva Júnior, E.N. Imidazoles and Oxazoles from Lapachones and Phenanthrene-9,10-dione: A Journey through their Synthesis, Biological Studies, and Optical Applications. *Chem. Rec.* **2021**, *21*, 2702–2738. [[CrossRef](#)]
45. Bagheri, M.; Mirzaee, M.; Hosseini, S.; Gholamzadeh, P. The photochromic switchable imidazoles: Their genesis, development, synthesis, and characterization. *Dye. Pigment.* **2022**, *203*, 110322. [[CrossRef](#)]
46. Ye, S.; Zhuang, S.; Pan, B.; Guo, R.; Wang, L. Imidazole derivatives for efficient organic light-emitting diodes. *J. Inf. Disp.* **2020**, *21*, 173–196. [[CrossRef](#)]
47. Tu, L.; Xie, Y.; Li, Z.; Tang, B. Aggregation-induced emission: Red and near-infrared organic light-emitting diodes. *SmartMat* **2021**, *2*, 326–346. [[CrossRef](#)]
48. Wang, K.; Wang, S.; Wei, J.; Miao, Y.; Zhang, Z.; Zhang, Z.; Liu, Y.; Wang, Y. Structurally simple phenanthroimidazole-based bipolar hosts for high-performance green and red electroluminescent devices. *RSC Adv.* **2015**, *5*, 73926–73934. [[CrossRef](#)]
49. Solomatina, A.I.; Kuznetsov, K.M.; Gurzhiy, V.V.; Pavlovskiy, V.V.; Porsev, V.V.; Evarestov, R.A.; Tunik, S.P.; Solomatina, A.I.; Kuznetsov, K.M.; Gurzhiy, V.V.; et al. Luminescent organic dyes containing a phenanthro[9,10- D]imidazole core and [Ir(N^ˆC)(N^ˆN)]⁺ complexes based on the cyclometalating and diimine ligands of this type. *Dalt. Trans.* **2020**, *49*, 6751–6763. [[CrossRef](#)] [[PubMed](#)]
50. Albrecht, M. Cyclometalation using d-block transition metals: Fundamental aspects and recent trends. *Chem. Rev.* **2010**, *110*, 576–623. [[CrossRef](#)] [[PubMed](#)]
51. Wang, Z.; Sun, Z.; Hao, X.-Q.; Niu, J.-L.; Wei, D.; Tu, T.; Gong, J.-F.; Song, M.-P. Neutral and Cationic NCN Pincer Platinum(II) Complexes with 1,3-Bis(benzimidazol-2'-yl)benzene Ligands: Synthesis, Structures, and Their Photophysical Properties. *Organometallics* **2014**, *33*, 1563–1573. [[CrossRef](#)]
52. Yoshida, M.; Kato, M. Regulation of metal–metal interactions and chromic phenomena of multi-decker platinum complexes having π -systems. *Coord. Chem. Rev.* **2018**, *355*, 101–115. [[CrossRef](#)]
53. Zhao, Q.; Huang, C.; Li, F. Phosphorescent heavy-metal complexes for bioimaging. *Chem. Soc. Rev.* **2011**, *40*, 2508–2524. [[CrossRef](#)]
54. Fernández-Moreira, V.; Thorp-Greenwood, F.L.; Coogan, M.P. Application of d6 transition metal complexes in fluorescence cell imaging. *Chem. Commun.* **2010**, *46*, 186–202. [[CrossRef](#)]
55. Thorp-Greenwood, F.L. An Introduction to Organometallic Complexes in Fluorescence Cell Imaging: Current Applications and Future Prospects. *Organometallics* **2012**. [[CrossRef](#)]
56. Solomatina, A.I.; Chelushkin, P.S.; Krupenya, D.V.; Podkorytov, I.S.; Artamonova, T.O.; Sizov, V.V.; Melnikov, A.S.; Gurzhiy, V.V.; Koshel, E.I.; Shcheslavskiy, V.I.; et al. Coordination to Imidazole Ring Switches on Phosphorescence of Platinum Cyclometalated Complexes: The Route to Selective Labeling of Peptides and Proteins via Histidine Residues. *Bioconjug. Chem.* **2017**, *28*, 426–437. [[CrossRef](#)] [[PubMed](#)]
57. Coogan, M.P.; Fernández-Moreira, V. Progress with, and prospects for, metal complexes in cell imaging. *Chem. Commun.* **2014**, *50*, 384–399. [[CrossRef](#)] [[PubMed](#)]
58. Stacey, O.J.; Ward, B.D.; Coles, S.J.; Horton, P.N.; Pope, S.J.A. Chromophore-labelled, luminescent platinum complexes: Syntheses, structures, and spectroscopic properties. *Dalt. Trans.* **2016**, *45*, 10297–10307. [[CrossRef](#)]

59. Vázquez-Domínguez, P.; Journaud, O.; Vanthuyne, N.; Jacquemin, D.; Favereau, L.; Crassous, J.; Ros, A. Helical donor–acceptor platinum complexes displaying dual luminescence and near-infrared circularly polarized luminescence. *Dalt. Trans.* **2021**, *50*, 13220–13226. [CrossRef]
60. Irmeler, P.; Winter, R.F. σ -Pt-BODIPY Complexes with Platinum Attachment to Carbon Atoms C2 or C3: Spectroscopic, Structural, and (Spectro)Electrochemical Studies and Photocatalysis. *Organometallics* **2018**, *37*, 235–253. [CrossRef]
61. Geist, F.; Jackel, A.; Irmeler, P.; Linseis, M.; Malzkuhn, S.; Kuss-Petermann, M.; Wenger, O.S.; Winter, R.F. Directing Energy Transfer in Panchromatic Platinum Complexes for Dual Vis–Near-IR or Dual Visible Emission from σ -Bonded BODIPY Dyes. *Inorg. Chem.* **2017**, *56*, 914–930. [CrossRef]
62. Horiuchi, S.; Moon, S.; Ito, A.; Tessarolo, J.; Sakuda, E.; Arikawa, Y.; Clever, G.H.; Umakoshi, K. Multinuclear Ag Clusters Sandwiched by Pt Complex Units: Fluxional Behavior and Chiral-at-Cluster Photoluminescence. *Angew. Chemie Int. Ed.* **2021**, *60*, 10654–10660. [CrossRef]
63. Shakirova, J.R.; Hendi, Z.; Zhukovsky, D.D.; Sokolov, V.V.; Jamali, S.; Pavlovskiy, V.V.; Porsev, V.V.; Evarestov, R.A.; Tunik, S.P. NIR emitting platinum pincer complexes based on the N⁴C ligand containing {benz[4,5]imidazo[1,2-a]pyrazin} aromatic system; synthesis, characterization and photophysical study. *Inorganica Chim. Acta* **2020**, *511*, 119776. [CrossRef]
64. Fleetham, T.; Golden, J.H.; Idris, M.; Hau, H.-M.; Muthiah Ravinson, D.S.; Djurovich, P.I.; Thompson, M.E. Tuning State Energies for Narrow Blue Emission in Tetradentate Pyridyl-Carbazole Platinum Complexes. *Inorg. Chem.* **2019**, *58*, 12348–12357. [CrossRef]
65. You, Y.; Kim, K.S.; Ahn, T.K.; Kim, D.; Park, S.Y. Direct Spectroscopic Observation of Interligand Energy Transfer in Cyclometalated Heteroleptic Iridium(III) Complexes: A Strategy for Phosphorescence Color Tuning and White Light Generation. *J. Phys. Chem. C* **2007**, *111*, 4052–4060. [CrossRef]
66. Na, H.; Lai, P.; Cañada, L.M.; Teets, T.S. Photoluminescence of Cyclometalated Iridium Complexes in Poly(methyl methacrylate) Films. *Organometallics* **2018**, *37*, 3269–3277. [CrossRef]
67. CrysAlisPro, Rigaku Oxford Diffraction, Version: 1.171.39.35a 2017.
68. Dolomanov, O.V.; Bourhis, L.J.; Gildea, R.J.; Howard, J.A.K.; Puschmann, H. OLEX2: A complete structure solution, refinement and analysis program. *J. Appl. Crystallogr.* **2009**, *42*, 339–341. [CrossRef]
69. Sheldrick, G.M. A short history of SHELX. *Acta Crystallogr. Sect. A Found. Crystallogr.* **2008**, *64*, 112–122. [CrossRef]
70. Sheldrick, G.M. Crystal structure refinement with SHELXL. *Acta Crystallogr. Sect. C Struct. Chem.* **2015**, *71*, 3–8. [CrossRef] [PubMed]
71. Spek, A.L. PLATON SQUEEZE: A tool for the calculation of the disordered solvent contribution to the calculated structure factors. *Acta Crystallogr. Sect. C Struct. Chem.* **2015**, *71*, 9–18. [CrossRef] [PubMed]
72. Brouwer, A.M. Standards for photoluminescence quantum yield measurements in solution (IUPAC Technical Report). *Pure Appl. Chem.* **2011**, *83*, 2213–2228. [CrossRef]
73. Suzuki, K.; Kobayashi, A.; Kaneko, S.; Takehira, K.; Yoshihara, T.; Ishida, H.; Shiina, Y.; Oishi, S.; Tobita, S. Reevaluation of absolute luminescence quantum yields of standard solutions using a spectrometer with an integrating sphere and a back-thinned CCD detector. *Phys. Chem. Chem. Phys.* **2009**, *11*, 9850–9860. [CrossRef]
74. Frisch, M.J.; Trucks, G.W.; Schlegel, H.B.; Scuseria, G.E.; Robb, M.A.; Cheeseman, J.R.; Scalmani, G.; Barone, V.; Petersson, G.A.; Nakatsuji, H.; et al. Gaussian 16 2016. Available online: <https://gaussian.com> (accessed on 28 April 2023).
75. Peverati, R.; Truhlar, D.G. Screened-exchange density functionals with broad accuracy for chemistry and solid-state physics. *Phys. Chem. Chem. Phys.* **2012**, *14*, 16187. [CrossRef]
76. Andrae, D.; Häußermann, U.; Dolg, M.; Stoll, H.; Preuß, H. Energy-adjusted ab initio pseudopotentials for the second and third row transition elements. *Theor. Chim. Acta* **1990**, *77*, 123–141. [CrossRef]
77. Tomasi, J.; Mennucci, B.; Cammi, R. Quantum Mechanical Continuum Solvation Models. *Chem. Rev.* **2005**, *105*, 2999–3094. [CrossRef] [PubMed]
78. O’boyle, N.M.; Tenderholt, A.L.; Langner, K.M. CCLIB: A library for package-independent computational chemistry algorithms. *J. Comput. Chem.* **2008**, *29*, 839–845. [CrossRef] [PubMed]
79. Martin, R.L. Natural transition orbitals. *J. Chem. Phys.* **2003**, *118*, 4775–4777. [CrossRef]
80. Lu, T.; Chen, F. Multiwfn: A multifunctional wavefunction analyzer. *J. Comput. Chem.* **2012**, *33*, 580–592. [CrossRef] [PubMed]

Disclaimer/Publisher’s Note: The statements, opinions and data contained in all publications are solely those of the individual author(s) and contributor(s) and not of MDPI and/or the editor(s). MDPI and/or the editor(s) disclaim responsibility for any injury to people or property resulting from any ideas, methods, instructions or products referred to in the content.